Science of the Total Environment 903 (2023) 166598

Contents lists available at ScienceDirect

Science of the Total Environment

journal homepage: www.elsevier.com/locate/scitotenv

Efficacy of green infrastructure in reducing exposure to local, traffic-related sources of airborne particulate matter (PM)

H.A. Sheikh [a,*], B.A. Maher [b], A.W. Woods [a], P.Y. Tung [a,c], R.J. Harrison [a]

[a] Department of Earth Sciences, University of Cambridge, Downing Site, CB2 3EQ, UK
[b] Center for Environmental Magnetism and Palaeomagnetism, University of Lancaster, LA1 4YQ, UK
[c] Department of Materials Science and Metallurgy, University of Cambridge, CB3 0FS, UK

HIGHLIGHTS

- Magnetic PM loading is dominated by superparamagnetic (<30 nm) Fe-oxide nanoparticles.
- Tredge leaves capture an estimated 23 % of local, traffic-derived PM_{10} emissions over two-day exposure period.
- Deposition and dispersion processes at the tredge reduce exposure to local, traffic-derived PM pollution.

GRAPHICAL ABSTRACT

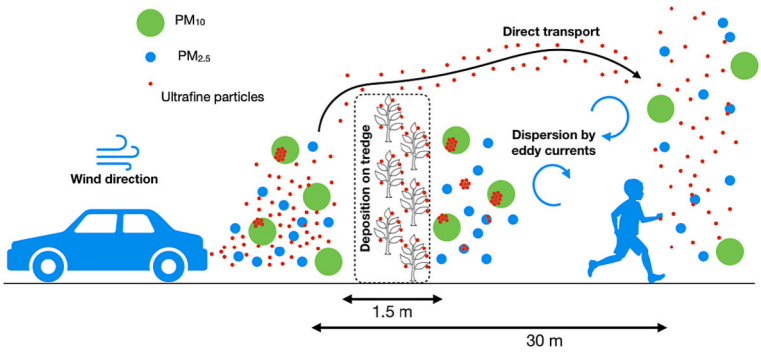

ARTICLE INFO

Editor: Elena Paoletti

Keywords:
Air pollution
Green infrastructure
Particulate matter
Vehicular pollution
Mitigation
Magnetism

ABSTRACT

One aim of roadside green infrastructure (GI) is to mitigate exposure to local, traffic-generated pollutants. Here, we determine the efficacy of roadside GI in improving local air quality through the deposition and/or dispersion of airborne particulate matter (PM). PM was collected on both pumped air filters and on the leaves of a recently installed 'tredge' (trees managed as a head-high hedge) at an open road environment next to a primary school in Manchester, U.K. The magnetic properties of PM deposited on leaves and filters (size fractions PM_{10} and $PM_{2.5}$) were deduced from hysteresis loops, first-order reversal curves (FORCs), and low-temperature remanence measurements. These were complemented with electron microscopy to identify changes in magnetic PM concentration downwind of the tredge/GI. We show that the tredge is permeable to airflow using a simple CO_2 tracer experiment; hence, it allows interception and subsequent deposition of PM on its leaves. Magnetic loadings per m^3 of air from filters (PM_{10} saturation magnetisation, M_s, at 5 K) were reduced by 40 % behind the tredge and a further 63 % in the playground; a total reduction of 78 % compared to roadside air. For the $PM_{2.5}$ fraction, the reduction in magnetic loading behind the tredge was remarkable (82 %), reflecting efficient diffusional capture of sub-5 nm Fe-oxide particles by the tredge. Some direct mixing of roadside and playground air occurs at the back of the playground, caused by air flow over, and/or through gaps in, the slowly-permeable tredge. The magnetic loading on tredge leaves increased over successive days, capturing ~23 % of local, traffic-derived PM_{10}. Using a heuristic two-dimensional turbulent mixing model, we assess the limited dispersion of PM <

* Corresponding author.
E-mail address: has57@cam.ac.uk (H.A. Sheikh).

https://doi.org/10.1016/j.scitotenv.2023.166598
Received 6 July 2023; Received in revised form 24 August 2023; Accepted 24 August 2023
Available online 25 August 2023

22.5 μm induced by eddies in the tredge wake. This study demonstrates that PM deposition on leaves reduces exposure significantly in this school playground setting; hence, providing a cost-effective mitigation strategy.

1. Introduction

The annual average concentration of airborne particulate matter (PM) for UK urban background environments has declined over the last 20 years. The concentration of $PM_{2.5}$ (particles <2.5 μm in aerodynamic diameter) decreased from 12.8 μg/m^3 in 2009 to 8.3 μg/m^3 in 2021 while PM_{10} (particles <10 μm in aerodynamic diameter) declined from 36.7 μg/m^3 in 1997 to 17.3 μg/m^3 in 2015 (Department for Environment, Food and Rural Affairs, 2022). Despite these lower average PM concentrations, there is no level of particulate air pollution that can be considered safe and new findings (e.g. Weichenthal et al., 2022) have found increased mortality rates on exposure to outdoor $PM_{2.5}$ concentrations <5 μg/m^3. In urban areas, exposure to traffic-related air pollution has been linked to adverse health outcomes, to which young children are especially vulnerable (Makri and Stilianakis, 2008; Rovelli et al., 2014; Schwartz, 2004; Sunyer et al., 2015). The spatial distribution of PM varies significantly according to location (Maher et al., 2022; Sanders et al., 2003; Yang et al., 2015), with major roads and industrial areas having different "mixes" of airborne pollutants, some of which are more harmful than others (Hammond et al., 2022).

Traffic-related pollution has two major sources: exhaust and non-exhaust emissions. Exhaust emissions consist of aerosols such as nitrogen oxides (NO_x), sulfur dioxide (SO_2), carbon dioxide (CO_2), carbon monoxide (CO), together with other primary pollutants including semi-volatile organic compounds and solid particles (PM of varied sizes and composition) comprising carbon and various metals such as Fe, Mn, Ni, Cr, Pb, and Pt (e.g., Birmili et al., 2006; Gonet and Maher, 2019). Non-exhaust emissions are dominated by wear of brakes (Sanders et al., 2003), tyres (Foitzik et al., 2018), road, and pavement surfaces (Gustafsson et al., 2008; Kupiainen et al., 2005). In the UK, brake-wear PM primarily comprises Fe, and is a source of trace metals such as Cu, Zn, Sb, Sn, S, and Ba (Gietl et al., 2010; Gonet et al., 2021b; Kukutschová et al., 2011; Sanders et al., 2003; Thorpe and Harrison, 2008). The 2016 emissions data from the UK's National Atmospheric Emissions Inventory (NAEI) indicated that non-exhaust emissions constituted the primary source of $PM_{2.5}$ (60 %) and PM_{10} (73 %) size fractions from road transport (Fussell et al., 2022). Previous studies in London, UK have estimated that traffic-related sources typically contribute around 20–48.5 % of the total measured ambient PM_{10} in roadside micro-environments (Harrison et al., 2021; Hicks et al., 2021).

Exposure to air pollution in urban settings can have adverse health effects on both children and adults at all life stages (i.e., including in the womb). According to epidemiological studies, exposure to air pollution can increase the risk of Alzheimer's (Anderson et al., 2012; Chen and Hoek, 2020; Pankhurst et al., 2008), dementia (Chen et al., 2017; Delgado-Saborit et al., 2021; Weuve et al., 2021), cardiovascular diseases (Brook et al., 2010; Newby et al., 2015; Schulz et al., 2005; Seaton et al., 1995), and respiratory diseases (Dockery and Pope, 1994; Dominici et al., 2006; Leitte et al., 2012). Children who commute and study in schools situated near busy roads are at risk of exposure to traffic-related air pollution, leading to negative health implications such as reduced cognitive development and ability (Sunyer et al., 2015). Children can spend a considerable amount of their time outdoors in schools (up to 24 % of their school time) (Tandon et al., 2018), where exposure to airborne PM from local traffic-related sources may be high.

It is essential, therefore, both to monitor and mitigate PM exposure in a range of urban settings. Green Infrastructure (GI) may provide a fast, and cost-effective solution that could assist in both these tasks. GI encompasses various green elements, including street trees, vegetation barriers (e.g., hedges, green walls), and green roofs. GI in cities has emerged as a promising urban planning solution for addressing air quality concerns, promoting sustainability (Irga et al., 2015; Kremer et al., 2015), mitigating the urban heat island effect (Gago et al., 2013; Tiwari et al., 2021), and making buildings more energy efficient (Pérez et al., 2014). Using GI such as trees, shrubs, hedges, and grass (Nowak et al., 2006) can reduce exposure to PM air pollution in local "hotspots" that affect vulnerable populations such as young children (Maher et al., 2013; Abhijith and Kumar, 2019; Kumar et al., 2019b; Lee and Maheswaran, 2011; Wang et al., 2019; Maher et al., 2022). Roadside GI influences local air quality through changes in airflow and resultant dispersion of particulate matter (PM), and/or by deposition of PM on its leaves. Well-designed GI next to heavily trafficked roads can potentially reduce particulate air pollution concentrations locally. However, depending on whether empirical or modelling approaches are taken, there is still considerable debate about the effectiveness of GI in reducing exposure to pollutants that may be hazardous to health.

Experimental studies have shown that roadside greening can play a role in airborne PM abatement strategies. Recent studies have found that green infrastructure in open (non-street canyon) environments can reduce PM concentrations by between 26 and 46 % for PM_1-$PM_{2.5}$ (Maher et al., 2022), 15–31 % for PM_{10}-PM_1 (Abhijith and Kumar, 2019) and another study found a 7 % and 9 % reduction in PM_{10} and $PM_{2.5}$ concentration, respectively, with a 21 % reduction in coarse PM (defined as $PM_{10-2.5}$) (Abhijith and Kumar, 2020). These claims have been explored and backed by experimental evidence where up to 50 % reduction in time-averaged PM concentration at roadside vegetation has been observed (Deshmukh et al., 2019; Ottosen and Kumar, 2020). PM concentration data has also been substantiated by empirical evidence from scanning electron microscopy and energy dispersive spectroscopy (SEM-EDS), suggesting that a higher percentage (up to 12 %) of traffic-related PM was deposited on leaves facing the roadside compared to the back of the hedge (Abhijith and Kumar, 2020). Magnetic proxies have also been used to study the PM deposition effectiveness of certain tree species. A previous study concluded that roadside vegetation can decrease indoor airborne PM concentrations of adjacent houses by >40 %, based on indoor PM measurements and magnetic and SEM-EDS analysis of newly installed roadside silver birch trees (Maher et al., 2013). Additionally, however, it has been proposed that specific types of vegetation can serve as a barrier to airflow and, as a result, limit the transportation of PM between traffic-related sources of pollutants and individuals present in nearby buildings (Al-Dabbous and Kumar, 2014; Kumar et al., 2019a; Maher et al., 2022, 2013; Tiwari and Kumar, 2022; Tomson et al., 2021). Overall, these studies indicate that the reduction in PM due to roadside vegetation, such as an up to 17 % reduction in $PM_{2.5}$ concentration in Istanbul (Ozdemir, 2019) or an up to 15 % reduction in PM_{10} behind the greenbelt in Wuhan (Chen et al., 2015), is a result of a combination of deposition and dispersion.

Conversely, studies based on computational fluid dynamic (CFD) modelling of the effect of roadside vegetation on airborne PM mostly indicate little air quality improvement. CFD-studies in Leicester city centre, U.K., on existing tall roadside trees found a reduction of 2.8 % for $PM_{2.5}$ as a result of deposition (Jeanjean et al., 2016) and a 7–9 % reduction due to dispersion of traffic emissions by changing the airflow (Jeanjean et al., 2016, 2015). It is important to note that Jeanjean et al. (2015, 2016) state that PM reductions are slightly more effective when trees are planted in open areas. However, placing trees upwind of local traffic-related emissions means much of the leaf canopy is distant from the local PM sources, making PM capture (via deposition) unlikely. Moreover, in their modelling, tree canopy heights are assumed to be as high as the buildings (18 m); tall trees reduce vertical airflow, resulting in increased near-ground PM concentrations (more pronounced in street canyons where emissions get trapped). Some CFD studies (Chen et al.,

2015; Hagler et al., 2012; Santiago et al., 2019, 2017) treat GI as impermeable barriers and conclude that solid barriers are more effective at reducing PM concentration on the downwind side as a result of re-routing airflow. However, this approach results in higher PM concentrations on the upwind roadside.

To understand the various sets of modelling scenarios that lead to discrepancies in the reported efficacy of roadside GI, it is important to note the different parameters that govern the deposition and aerodynamic effects of vegetation and changes in airflow. The two key parameters that cause variations in determining efficacy of GI (Abhijith et al., 2017; Beckett et al., 2000; Janhäll, 2015; Maher et al., 2022) are 1) vegetation (height, location, species, design, permeability) and 2) depositional velocity ($V_d = F/C$, where F = particle flow rate in μg m^{-2} s^{-1} and C = particle concentration in μg m^{-3}). V_d also varies with plant species, leaf size, morphology, and density (Beckett et al., 2000; Mitchell et al., 2010; Zhang, 2001). According to a CFD modelling study performed in an avenue (i.e., a street not surrounded by buildings) (Santiago et al., 2019), the characteristics of vegetation structure (combination of leaf area density and mix of hedge and trees, etc.) were most important in reducing black carbon (BC) concentrations downwind by up to 66 % (dependent on value of V_d used). GI with higher leaf area density helps create a turbulent flow for pollutant dilution, whilst also offering greater leaf surface area for particle impaction and deposition (Tiwari and Kumar, 2022), which explains greater PM deposition efficacies from denser vegetation. Moreover, the aerodynamic contribution of vegetation is dependent on the prevailing wind direction which, in certain cases, can impede airflow, leading to higher concentrations of air pollutants (Buccolieri et al., 2011). The different 'standard' V_d values e.g., 1) 0.02 cms^{-1} value for dry deposition of aerosols (Peters and Eiden, 1992) (Vos et al., 2013) or 2) 0.64 cms^{-1} for $PM_{2.5}$ (Nowak et al., 2006) commonly under-represent actual, species-specific V_d values and hence force a relatively low depositional estimate and proportionally greater effect of airflow modification (Maher et al., 2022). Conversely, when modelling studies use higher V_d values, significant improvement in air quality has been simulated (Maher et al., 2022; Mitchell et al., 2010; Pugh et al., 2012; Santiago et al., 2017; Tallis et al., 2011; Wang et al., 2019).

Hence, the impact of GI on air quality in roadside environments can be both positive and negative depending on the interactions between the GI and air pollution in the local air flow, as well as site-specific factors such as the design of the GI and road width and height/scale of adjacent buildings (Abhijith et al., 2017). Previous studies have looked at air flow and pollutant transport in a built environment concluding that porous and solid barriers can improve air quality and GI parameters such as tree crown height, plant height, leaf density, and tree/plant spacing influences air quality improvement (Gallagher et al., 2015). Studies have also suggested that the vegetation has to be dense enough to allow deposition of PM on leaves but permeable enough to allow smoother airflow through it, concluding the need for careful designing of GI (Janhäll, 2015).

The primary goal of this study was to use observational data from field measurements, and complementary independent analyses, to examine the impact of GI on reduction of local, traffic-derived PM pollution. Here, we build on a previous study done at St Ambrose primary school in Manchester, U.K. (Maher et al., 2022) to investigate further the efficacy of newly installed GI, 'tredges' (trees managed as head-high hedges) for PM removal at heavily trafficked roadsides. We present observational evidence of PM deposition on leaves and test the tredge's permeability. Using a combination of magnetic and microscopy methods, we quantify the amount of local, traffic-derived PM deposited on leaves. We also present a heuristic two-dimensional turbulent mixing model to show how differently sized PM is dispersed in the lee/wake of the tredge. The main objectives of this study are to (1) quantify PM at the roadside, immediately behind the tredge, and at the back of the playground (30 m from the road) over a 5-day sampling period using traditional gravimetric and magnetic methods; (2) examine, using electron microscopy, the composition of the PM at the roadside, behind the tredge, and deposited on leaves; (3) quantify the magnetite concentration in the roadside and school side air and examine the magnetic PM at the roadside and on leaves; (4) quantify the removal of previously deposited PM from leaves by rainfall and by artificially washing the tredge; (5) demonstrate the permeability of the tredge to airflow using a novel CO_2 tracer experiment, and (6) determine the combined effects of dispersion and deposition in reducing exposure to traffic-derived PM in an open environment via GI.

2. Materials and methods

2.1. Air sampling

The study site (Supplementary Fig. S1) is located at St Ambrose Primary School, Manchester, immediately adjacent (i.e., within 1.5 m) of Princess Road (average 80,000 vehicles/day). We installed air sampling pumps at four locations: (A) at the roadside (wire perimeter fence, no tredge), (B) on the roadside of the recently installed (July 2019) western red cedar tredge (deliberate selection based on efficient capturing of airborne ultrafine particles (UFPs) (Maher et al. (2022)); (C) on the school side of the tredge; (D) at the back of the school playground (~30 m from the road). Airborne PM was collected using the "filter packs" technique (Allen et al., 1997). Two filter packs were used: (1) a 47 mm, 12 μm pore size Nuclepore polycarbonate pre-filter collected coarse mode particles having an aerodynamic diameter > 2.5 μm) and (2) 47 mm, 1 μm PTFE filter located downstream of the pre-filter collected the remaining fine and ultrafine particles. The sampling pumps (Charles Austen Pumps Ltd., Byfleet, U.K., model LD30) were equipped with gas meters (Schlumberger gas meters Gallus 2000). By running the pumps at 20 L/min, the PM size cut-off for the first filter was at 2.5 μm. Particles <2.5 μm passing through the polycarbonate filter are trapped on the PTFE filter. Hereafter, we refer to the PM on the polycarbonate filters as PM_{10} and on the PTFE filters as $PM_{2.5}$.

The pumps were run for five working days, between Monday 10/05/22 and Friday 14/05/22, for a 9.5 h interval from 0730 to 1700 to measure PM at this heavily trafficked site during the morning and evening rush hours. Following the sampling campaign, filters were placed in polyethylene bags and refrigerated. For gravimetric analysis, the mass of collected material was determined by weighing the blank filters before and after the sampling campaign using a Mettler AT250 microbalance (with 0.01 mg precision). The filters were conditioned in a climate-controlled room at a temperature of 20 °C and humidity level of 50 % for 24 h before weighing. The filters were allowed to stabilise in the balance room and the mass values recorded after the number had stabilised.

2.2. Leaf sampling

On Day 1, to try to 're-zero' the amount of PM already deposited on the leaves of the western red cedar tredge, we washed the hedge evenly with a hosepipe for 5 min. Leaf samples were collected on Day 1 (10/05/22) at 0700 at inhalation height for children (1 m) across three different locations on both the roadside and school side of the tredge. In total, 3 samples were collected on each side of the tredge. Additional leaves were collected on Day 3 (12/05/22) at 0730, after rainfall which began at 0500 and continued until 1230. Leaves were collected again on Day 5 (0730, 14/05/22). The surface areas of the leaves were determined using a scanner, to normalize each measured magnetic parameter.

2.3. Room-temperature magnetic granulometry

For quantification and comparison of magnetic PM loading on the air filters and leaves, all samples were analysed for their bulk magnetic properties at the Centre for Environment Magnetism and Palaeomagnetism (CEMP), Lancaster University. To estimate the amount of

stable single-domain ferrimagnetic particles (~25–80 nm), anhysteretic remanent magnetization (ARM) was measured. A Molspin AF demagnetizer (with DC attachment) was used to impart an ARM in an 80 milliTesla (mT) alternating current (AC) field and 100 μT direct current (DC) bias field. ARM susceptibility (χ_{ARM}) was calculated by dividing ARM by the DC bias field. To measure the total concentration of remanence-carrying ferrimagnetic particles (> ~ 25 nm) of our samples, room-temperature saturation isothermal remanent magnetization (SIRM) was acquired at 1 T using a Newport electromagnet. All our room temperature remanence measurements were made on an AGICO JR-6A magnetometer (sensitivity 2.4 × 10^{-6} Am^{-1}).

2.4. Low-temperature magnetic measurements

To quantify the concentration of superparamagnetic (SP) particles (<~25 nm), we performed low-temperature SIRM measurements on leaves and filter samples collected from either side of the tredge, using a Quantum Design Magnetic Property Measurement System (MPMS) at the Maxwell Centre, University of Cambridge. We measured room-temperature SIRM (RT-SIRM) warming and cooling curves, zero-field cooled (ZFC), and field-cooled (FC) curves to confirm the magnetic mineralogy of our samples. We also measured room-temperature (300 K) and low-temperature (5 K) hysteresis loops to quantify the mean magnetite content in our samples.

2.5. Hysteresis loops and first-order reversal curves (FORCs)

Hysteresis loop and FORCs can be used to determine bulk magnetic variations in samples. Room (300 K) and low (5 K) temperature hysteresis loops for filter B, C, and D were acquired on the MPMS and the M_s value was obtained from each loop and used as a magnetic proxy. All FORCs were measured on a LakeShore Vibrating Sample Magnetometer (VSM) Series 8600 at the Department of Materials Sciences, University of Cambridge except for the leaf sample. FORCs were measured on four PM_{10} filters, one $PM_{2.5}$ filter, and one roadside leaf sample (measured on the Princeton Micromag 2900 Alternating Gradient Magnetometer). 513 FORCs were acquired for each sample in discrete mode using field steps of 1 mT and an averaging time of 300 ms. FORC diagrams were processed with the FORCinel software (Harrison and Feinberg, 2008) using VARIFORC smoothing (Egli, 2013).

2.6. CO_2 tracer experiment

CO_2 tracer experiments are normally used in indoor environments; however, we simulated air (+ airborne PM) flow using a CO_2 fire extinguisher as a tracer gas to measure the airflow rate along and through the installed tredge. 18 CO_2 monitors were placed along parallel and perpendicular profiles of the tredge to detect gas concentrations (3 failed to register any data) (Supplementary Fig. S3). During the experiment, 16 pulses of CO_2 were released, each lasting 2–3 s, at different positions both parallel and perpendicular to the tredge and the evolving concentration of CO_2 was measured using the array of monitors. An anemometer was placed on each side of the hedge to measure the mean wind direction and speed.

2.7. Modelling particle flow across the hedge

To model the flow, mixing, and fall out of the particles, we present a simplified model to capture the length scale over which we expect significant dilution (by mixing with 'cleaner' air behind the tredge) and settling to occur. Eddies are generated by wind deflected over the tredge (we assume impermeable tredge in this simplified model). This leads to the evolution of the particle concentration according to the following relation downwind of the tredge (Cushman-Roisin and Beckers, 2011):

$$u\frac{\partial c}{\partial x} - v\frac{\partial c}{\partial y} = \frac{\partial}{\partial y}\left(D\frac{\partial c}{\partial y}\right) \tag{1}$$

where x and y are the downwind distance and height, respectively, of the tredge (Supplementary Fig. S2), v = fall velocity (ms^{-1}), c = concentration (kgm^{-3}), D = eddy diffusivity (m^2s^{-1}), $\underline{u}$ = wind speed (ms^{-1}). In terms of particle settling, the fall speed (v) of the particle is given by Stokes' law:

$$v = \frac{2gr^2\rho_p}{9\mu_A} \tag{2}$$

where g is gravity at 9.81 ms^{-2}, ρ_p= particle density (kgm^{-3}), r = particle radius (m), μ_A= viscosity of air (1.8 × 10^{-5} kgm^{-1} s^{-1}). We can model the eddy diffusivity, in terms of u, the wind speed, and h, the tredge height, noting that the diffusivity falls to zero near the ground, so it has the form:

$$D \sim 0.1uhf\left(\frac{y}{h_b}\right)$$

where the coefficient 0.1 relates to the eddy speed being a fraction of the wind speed u, and the function $f\left(\frac{y}{h_b}\right)$ has value $f = 1$ for $y > h_b$ and falls to zero as $y \to 0$, h_b is the depth of the boundary layer near the ground where the turbulent diffusion falls to zero. To make progress, it is convenient to take a vertical integral and this leads to the relation for the net horizontal flux of particles of concentration c, given by f as:

$$\frac{df}{dx} = u\frac{d}{dx}\int_0^H c\,dy = -vc_0 \tag{3}$$

Where $H \gg h$ and $c(H) = \frac{dc}{dy}|_H = 0$.

Since the horizontal length scale over which the particles settle is much greater than the tredge height, owing to the small fall speed compared to the wind speed, we expect that after some mixing the vertical extent of the particle-laden flow will be of the depth scale $\left(\frac{D}{v}\right)$ and the flux of the particles scale as $f \sim \frac{uD}{v}c(x,0)$. We deduce that the concentration decays downwind of the tredge according to:

$$\frac{dc}{dx}(x,0) = -\frac{v^2}{Du}c(x,0) \tag{4}$$

and solving it,

$$c(x,0) \cong c(0,0)exp^{\frac{-v^2x}{Du}} \tag{5}$$

where $\left(\frac{D}{v}\right) \sim \frac{0.1uh}{v}$ is the depth of the flow. For concentration decay we assumed a windspeed of 3 ms^{-1} from our windspeed data and h = 1.5 m.

2.8. Electron microscopy

Scanning electron microscopy (SEM) was performed on PM_{10} and $PM_{2.5}$ roadside filters and a leaf sample using a Thermo Fisher Quanta-650F SEM. Samples were mounted on an SEM stub and carbon coated to prevent charging. All backscatter electron (BSE) imaging and energy dispersive x-ray spectroscopy (EDS) were done at an accelerating voltage of 15 kV. Samples for transmission electron microscopy (TEM) were prepared by placing a PTFE filter ($PM_{2.5}$) in a 3 ml Eppendorf tube and displacing particles by ultrasonicating the suspension for 60 s in distilled water. A micropipette was used to take a few drops of the suspension onto a copper TEM grid and left to dry overnight. TEM was performed on a Tecnai Osiris FEG TEM at an accelerating voltage of 200 kV; collecting TEM high-angle annular dark-field (HAADF) imaging in scanning transmission electron microscopy (STEM) mode, and EDS maps were collected using 4 Bruker silicon drift detectors (SDD).

3. Results

3.1. Spatial variation in PM mass concentrations

For the sampling period 09/05/2022 to 13/05/2022 (0730–1700 every day), the measured PM_{10} concentrations at each sampling site exceeded the World Health Organisation (WHO) annual mean limit of 15 μg/m^3. The PM_{10} concentration for Site A (roadside, no tredge) averaged 26 μg/m^3, Site B (roadside of the tredge) averaged 21.7 μg/m^3, Site C (school side of the hedge) averaged 19.7 μg/m^3, and Site D (back of the playground, ~30 m from the road) averaged 18.2 μg/m^3. $PM_{2.5}$ concentrations at Sites A, B, and C were similar at 5.0 μg/m^3, 6.1 μg/m^3 (the same as 5-month average of 6.1 μg/m^3 in the previous study (Maher et al., 2022) and 5.9 μg/m^3, respectively; at Site D, it was about 3 × less and averaged 2.4 μg/m^3 (Fig. 2).

Over the 5-day averaged sampling period, the school side of the tredge (Site C) is 9 % and 3 % lower in PM_{10} and $PM_{2.5}$ concentrations, respectively from roadside locality. In comparison, $PM_{2.5}$ reduction at Site C was ~15 % in the previous study (Maher et al., 2022) compared with the roadside location (Fig. 1). At playground Site D (~30 m from the road), PM_{10} and $PM_{2.5}$ concentrations are 23 % and 60 % lower, respectively, compared with Site B (roadside, tredge).

The airborne PM concentrations measured in urban environments comprise a background 'regional' PM component in addition to any local, e.g., traffic-related, PM increment. PM_{10} and $PM_{2.5}$ background concentration data were obtained from the Manchester Supersite (real-time measurements using Palas FIDAS200 at the Firs Environmental Research Station, Fallowfield Campus, Manchester). The local, traffic-derived PM_{10} increment could thus be estimated as ~40 % at Site A (w/o tredge), 29 % at Site B (roadside, tredge), 21 % at Site C (school side, tredge) and 17 % at Site D (playground). The local $PM_{2.5}$ increment constituted 66 % at Site A (w/o tredge), 67 % at Site B (roadside, tredge), 60 % at Site C (school side, tredge) and 16 % at Site D (playground).

3.2. Magnetic PM concentration on air filters

In previous studies, the amount of magnetic PM deposited on roadside leaves has been used as a proxy for temporal and spatial variations of airborne PM (Hansard et al., 2012, 2011; Hofman et al., 2014a; Matzka and Maher, 1999; Mitchell and Maher, 2009; Sheikh et al., 2022) and to estimate magnetite grain size variations. Similarly, in this study, the magnetic signal is primarily used as a proxy for locally generated, magnetically enriched traffic-related PM. All magnetic measurements of air filter samples are normalised to a unit volume (1 m^3) of air sampled.

3.3. Spatial variation in RT-SIRM proxy

Room-temperature SIRM (RT-SIRM) indicates the total contribution of stable remanence carriers (magnetic PM) at 300 K (Fig. 2). The measured RT-SIRM value for the PM_{10} filter from the roadside of the tredge (Site B) is 4.44 × 10^{-10} Am^{-1}, 3.33 × 10^{-10} Am^{-1} (i.e., 25 % lower) at the school side of the tredge (Site C), and 1.79 × 10^{-10} Am^{-1} (60 % lower) at back of the playground (Site D) (Fig. 2A).

For the $PM_{2.5}$ filters, the RT-SIRM values are 2.68 × 10^{-10} Am^{-1} at Site B, and 6.79 × 10^{-11} Am^{-1} at Site C, making a 75 % reduction on the school side of the tredge. At the playground (Site D), the value is 9.50 × 10^{-11}, slightly higher than Site C, but 65 % lower than the roadside Site B (Fig. 2B).

3.4. Spatial variation in LT-SIRM proxy

By measuring low-temperature SIRM (LT-SIRM at 5 K), the remanence contribution is captured from very fine ferrimagnetic particulates (<~25 nm) that are otherwise thermally unstable at room temperature. For the PM_{10} filters, the LT-SIRM value is highest at the roadside, 39 % lower at the school side of the tredge and 82 % lower at the playground (Fig. 2C). For the $PM_{2.5}$ filters, roadside and behind-tredge LT-SIRM values are 1.47 × 10^{-9} Am^{-1} and 5.11 × 10^{-10} Am^{-1} respectively, marking a 65 % reduction in magnetic PM on the school side of the tredge. At the playground site, the LT-SIRM value is 4.91 × 10^{-10}, 67 % lower than at the roadside of the tredge and 4 % lower than the school side of the tredge (Fig. 2D).

3.5. Spatial variation with χ_{ARM} proxy

Room-temperature ARM measurements are sensitive to the concentration of ultrafine stable single-domain particles (~25–80 nm) (Maher, 1988). Normalising the filter χ_{ARM} values for pumped air volume, there is a 46 % reduction in the PM_{10} χ_{ARM} value from the roadside to behind the tredge, and a 60 % reduction between the roadside and the playground (Supplementary Fig. S4). For the $PM_{2.5}$ filters, values for the

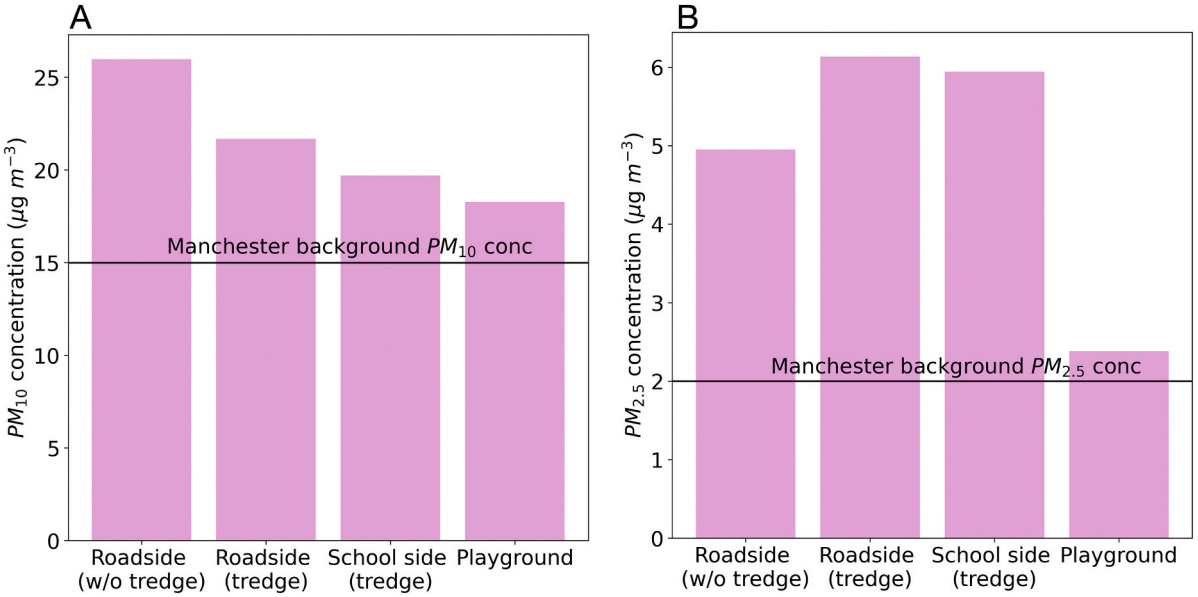

Fig. 1. (a) PM_{10} and (b) $PM_{2.5}$ concentrations measured at the four sampling sites. All pumps were switched on from 07:30 to 17:00 every day for five sampling days.

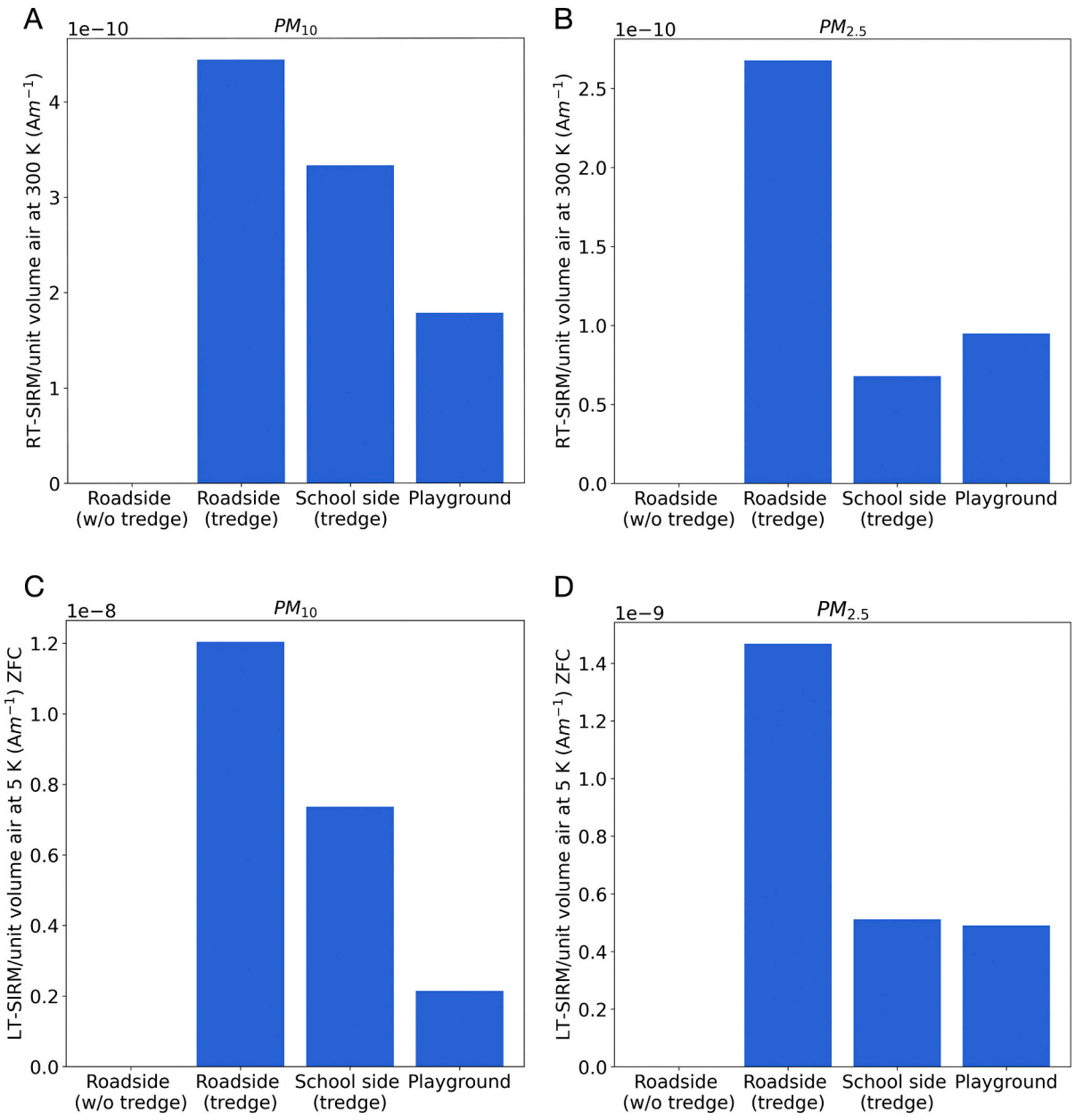

Fig. 2. SIRM per m^3 of air for PM_{10} and $PM_{2.5}$ filters measured at room-temperature (A, B) and 5 K (C, D). Data is presented for Sites B–D. Site A was not measured.

roadside and behind-tredge sites are 2.68×10^{-4} and 2.01×10^{-4} respectively, marking a 25 % reduction on the school side of the tredge. At the playground site (~30 m from the road), the χ_{ARM} is 24 % higher than Site A (roadside w/o tredge) and 99 % higher than Site B (roadside with tredge).

3.6. Spatial variation with M_s as a proxy

Saturation magnetisation (M_s) is a measure of the total contribution from ferrimagnetic PM. The value of M_s at 300 K and at 5 K for PM_{10} decreases by 87 % and 78 % respectively at the playground compared to the roadside tredge (Fig. 3A and B). Similarly, M_s at 5 K for $PM_{2.5}$ from the roadside to the school side of the tredge drops by 82 % but registers an increase at the playground by 17 % (Fig. 3D) compared to roadside tredge. Cumulative M_s ($PM_{10} + PM_{2.5}$) at 5 K value decreases by 48 % and 64 % at the school side of tredge and playground, respectively, compared with the roadside of the tredge (Fig. 3F).

Moreover, in low-temperature (5 K) measurements (Fig. 3B, D, F), the M_{rs}/M_s value (obtained from hysteresis data, Supplementary Fig. S5) of between 0.08 and 0.2 for the playground and roadside sites demonstrates the presence of superparamagnetic particles <5 nm, while an M_{rs}/M_s value of 0.55 observed on the school side of the tredge indicates only single-domain particles >5 nm are present.

3.7. Magnetite weight% on filters

RT- and LT-saturation magnetisation measurements can be used to estimate the proportion of magnetite in the total mass of PM_{10} and $PM_{2.5}$. Assuming the dominant iron-oxide phase is magnetite, by taking the experimental M_s value and dividing by the theoretical M_s value for magnetite, we can estimate the mass of magnetite on each filter. Subsequently, this is divided by the total dust mass on the filters to get magnetite weight % (Supplementary Table S2). Our low temperature calculations show that magnetite wt% estimates for the PM_{10} filter and $PM_{2.5}$ filter at Site B is 1.7 % and 1.2 %, respectively; Site C: PM_{10} (1.4 %) and $PM_{2.5}$ (0.2 %); Site D: PM_{10} (0.5 %) and $PM_{2.5}$ (4.1 %).

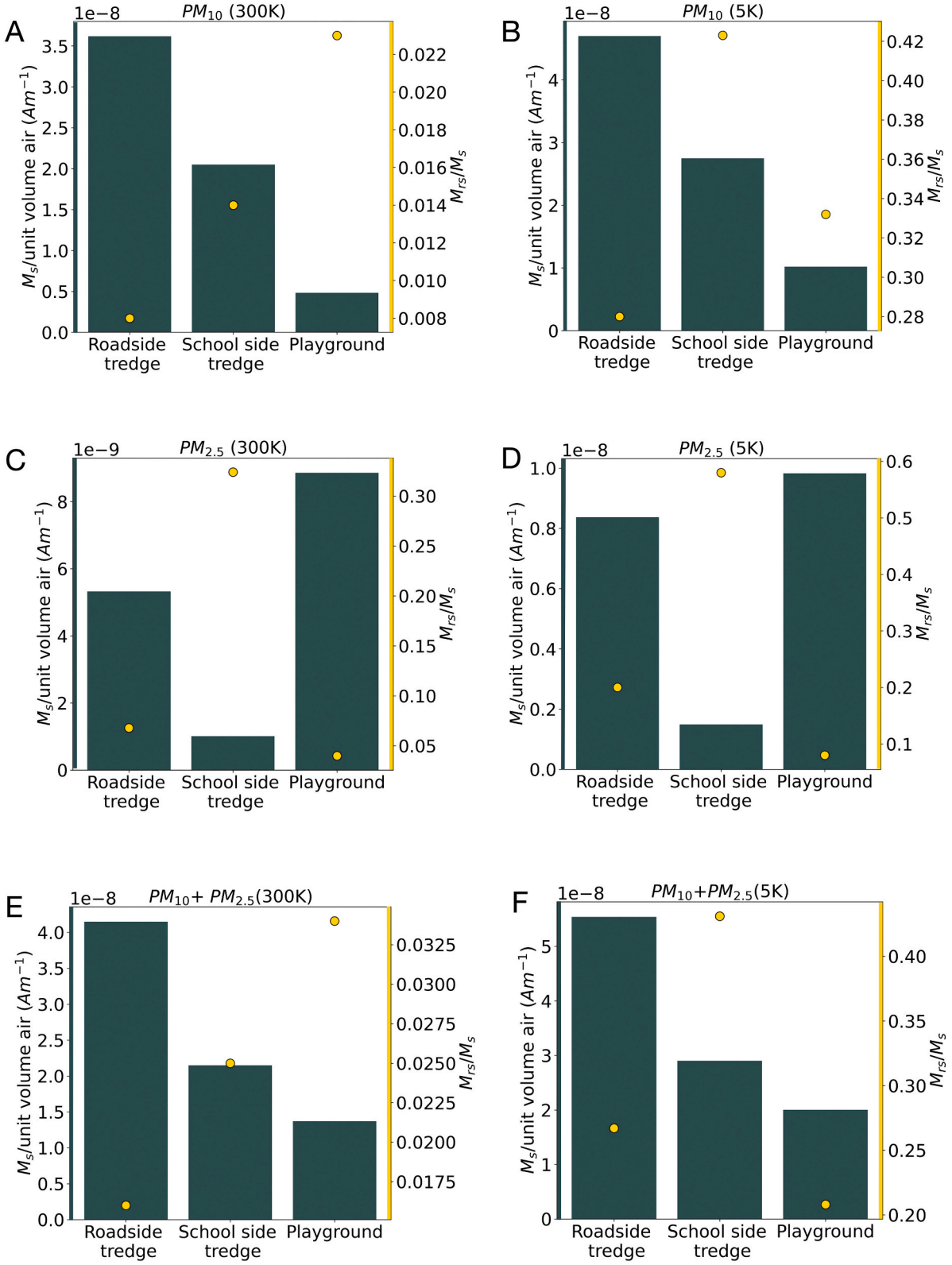

Fig. 3. Saturation magnetisation per m^3 of air (M_s) (bars) and M_{rs}/M_s ratio (yellow circles) for Sites B–D at 300 K (A, C, E) and 5 K (B, D, E). Data are shown for PM_{10} (A, B), $PM_{2.5}$ (C, D) and for the sum of both PM_{10} and $PM_{2.5}$ (E, F).

3.8. Magnetic concentration on leaves

The total amount of magnetic PM deposited on the tredge leaves was quantified by measuring leaf area-normalised RT-SIRM (Fig. 4) for roadside and school side localities of the tredge. Artificially washing the tredge for 5 min with a hose was effective in reducing the RT-SIRM values by between 7 and 30 % (Fig. 4A) - this gave us a reference RT-SIRM value to compare further sampling data. After exposing leaves for two days (i.e., 2 days after washing the tredge), leaves collected on Wednesday from the roadside have significantly higher SIRM values

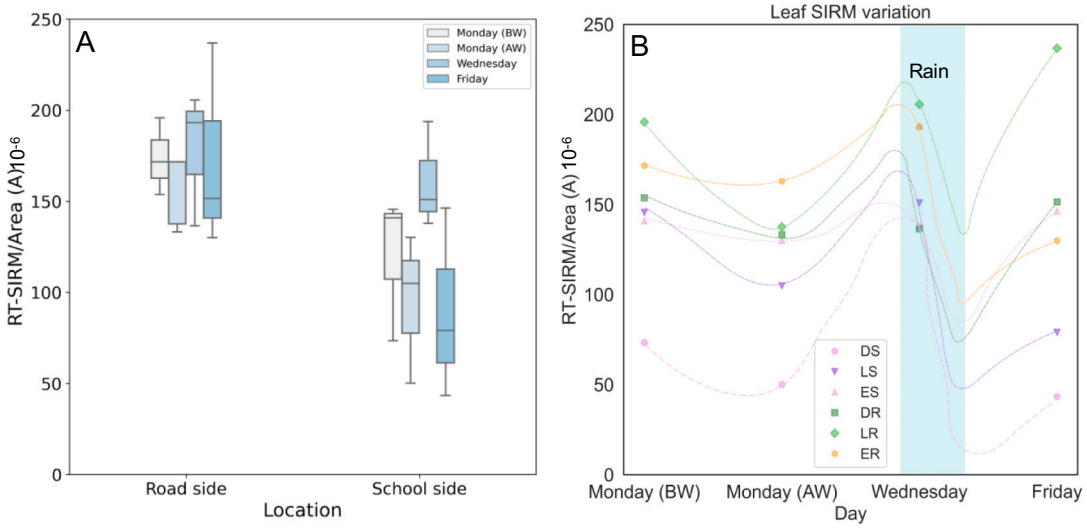

Fig. 4. (A) spatial and (B) temporal variation in RT-SIRM (normalised to leaf surface area) on roadside and school side locations of the tredge on different sampling days. BW: Before Washing; AW: After Washing. Sampling was done at 7 30 am on each day. DS (dense vegetation), LS (low vegetation), ES (edge of the tredge) refer to school side, while DR, LR, ER refer to roadside leaf sampling locations. The dotted line is a subjective guide to the eye showing the likely variation in SIRM over the 5-day sampling campaign.

than those from the school side (Fig. 4A and B), demonstrating active deposition of magnetic particles on the tredge. On Wednesday, RT-SIRM/area values for the roadside ranged between 137 $\times$ 10^{-6} A and 298 $\times$ 10^{-6} A, with an average of 211 $\times$ 10^{-6} A; school side leaves had slightly lower magnetic loading, ranging between 93 $\times$ 10^{-6} A and 275 $\times$ 10^{-6} A, with an average of 175 $\times$ 10^{-6} A. The rainfall event on Wednesday washed off PM from the leaves' surface, likely to have lowered the SIRM signal by anywhere between 50 and 70 % (Xu et al., 2017). On Friday, RT-SIRM values for all leaves were lower than those recorded on Wednesday (between 24 and 69 % lower) except for two roadside localities—DR (dense vegetation) and LR (less dense vegetation) which were 10 % and 15 % higher than on Wednesday (Fig. 4B).

Following (Maher et al., 2022) we used the leaf magnetic loadings to estimate that ~23 % of local, traffic-derived PM_{10} was removed by deposition on the tredge (Supplementary Table S4).

3.9. Magnetic particle size and composition on the filters and leaves

An estimate of the superparamagnetic (SP) contribution in our samples was calculated by comparing the LT-$SIRM_{ZFC}$ at 10 K to the RT-SIRM at 10 K. This measure provides an estimate of particles which are not capable of holding remanence when magnetized at room temperature (unblocked SP) but can hold a remanence when cooled to 10 K (blocked SP). The SP fractions in our PM_{10} and $PM_{2.5}$ filters for pumps B and C comprise around 99 % and 90 % of the total remanence-carrying particles at 5 K (Table 1). Previously, similarly high SP contributions of up to 88 % have been reported in roadside PM (Sagnotti et al., 2006; Saragnese et al., 2011) and in brake wear-derived PM (Gonet et al., 2021b).

Leaf sample (LR02) and filters (BT, CT, DT etc.) (Supplementary Fig. S6) showed some evidence of dampened Verwey transition at around 110 K (lower temperature than expected for stoichiometric magnetite (125 K). This dampened signature has been associated with surface-oxidised magnetite due to maghemitization process in previous studies (Özdemir et al., 1993; Özdemir and Dunlop, 2010).

3.10. Microscopy

3.10.1. PM on air filters and leaf surface

Scanning electron microscopy (SEM) and energy dispersive spectroscopy (EDS) data show that the ambient PM is dominated by irregularly shaped non-anthropogenic silicate minerals, salt, and anthropogenic (traffic-related) metal-oxide particles (such as Fe-oxide) (Fig. 6). Most of the non-anthropogenic particles are between 1 μm and 15 μm; traffic-related particles are much finer and on average are in the <2.5 μm size fraction. EDS data for the leaf sample shows that its surface-deposited PM consisted mostly of C, Si, Ca, Na, and Fe. Transmission electron microscopy (TEM) (Fig. 5) shows that the Fe-bearing nanoparticles (<20 nm) occur both discretely (1–10 nm) and as agglomerated clusters (up to 5 μm). EDS maps from high-angle annular dark-field (HAADF) imaging in scanning transmission electron microscopy (STEM) mode confirms the presence of abundant rounded Fe-oxide nanoparticles with an aspect ratio of >0.9 and sizes <5 nm, which are small enough to remain superparamagnetic at 5 K.

3.10.2. FORC fingerprints of magnetic PM

Our SEM and FORC data (Supplementary Fig. S7) suggest that most of the magnetic PM on the leaves is dominated by particles <2.5 μm. The FORC diagrams (Supplementary Fig. S7) confirm the presence of SP, SD, and vortex/pseudo single domain behaviour. According to micromagnetic simulations of Lanci and Kent (2018), we attribute the peak at the origin to a viscous SP component. The samples also show evidence of

Table 1
SP particle contribution to the magnetic PM on the PM_{10} and $PM_{2.5}$ filters.

St. Ambrose School	PM_{10}			$PM_{2.5}$		
9–13.05.2022	LT-$SIRM_{ZFC\text{-}5K}$ (Am^2)	RT-$SIRM_{5K}$ (Am^2)	SP %	LT-$SIRM_{ZFC\text{-}5K}$ (Am^2)	RT-$SIRM_{5K}$ (Am^2)	SP %
A (roadside, no tredge)	–	–	–	–	–	–
B (roadside, tredge)	5.90E-07	1.47E-09	99.8	7.18E-08	8.24E-09	88.5
C (school side, tredge)	4.71E-07	3.25E-09	99.3	3.27E-08	3.25E-09	90.1
D (playground)	1.08E-07	3.68E-09	96.6	2.47E-08	2.00E-09	91.9

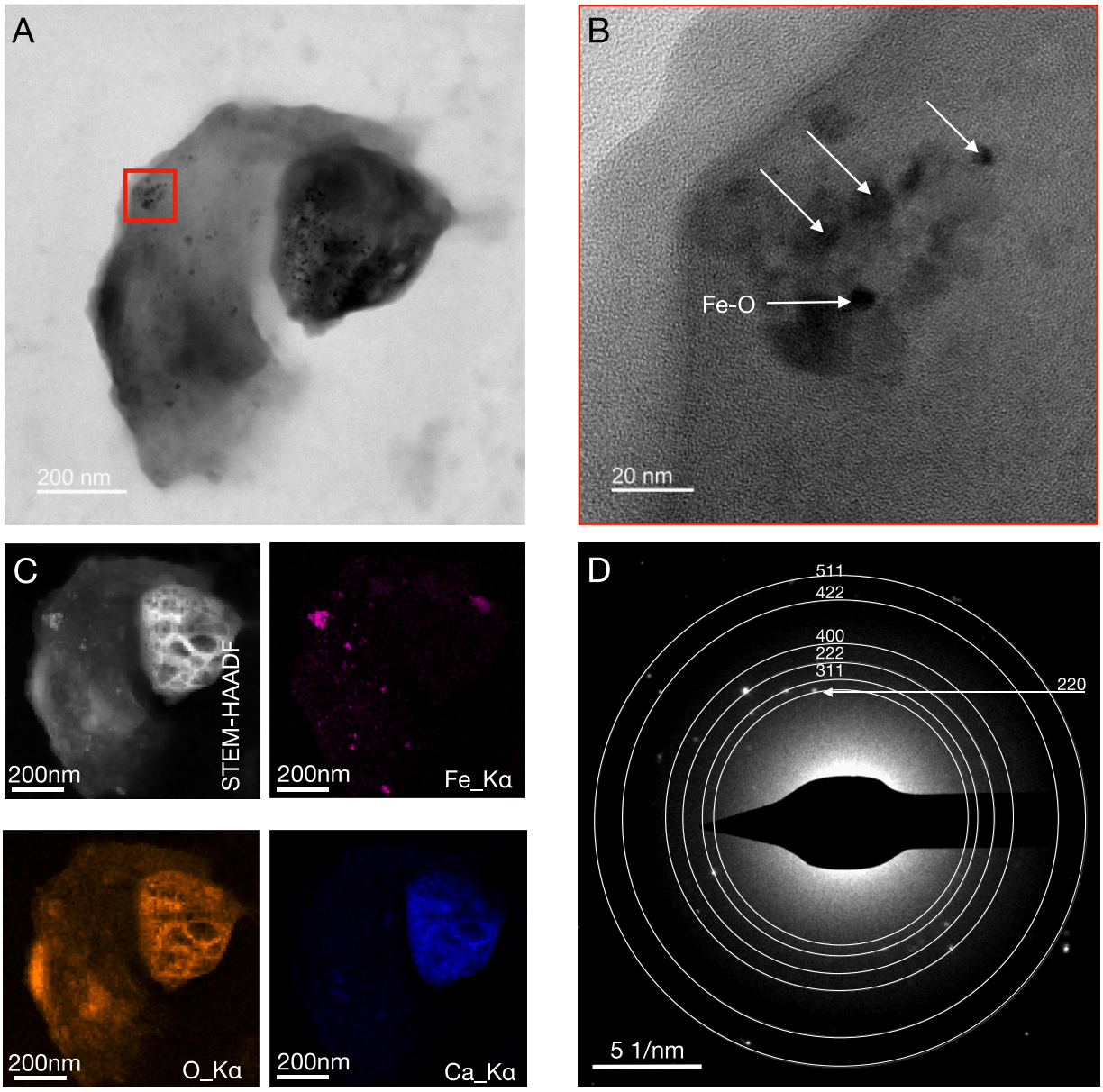

Fig. 5. (A) Transmission electron microscopy (TEM) bright-field (BF) image showing Fe-oxide nanoparticles (<20 nm) embedded in a larger particle; (B) zoomed in image showing nanoparticles <5 nm in diameter; (C) energy dispersive x-ray spectroscopy (EDS) elemental maps for Fe and O; (D) selected area diffraction (SAED) pattern showing randomly oriented magnetite crystals.

a tail extending to higher coercivities (B_C) of up to 150 mT, which suggests the additional presence of SD grains. Previous FORC roadside signatures have assigned diverging contours from the origin, along the B_u axis to a strong multi-domain (MD) signal (Sagnotti et al., 2009; Winkler et al., 2022, 2021), or a weaker MD signal as reported in Sheikh et al. (2022). However, the lack of a strong MD signal in the leaf FORCs of Sheikh et al. (2022), despite the presence of >5 μm spherule particles observed in microscopy, was explained by the dendritic form of the spherules, which is likely to reduce the effective grain size to <1 μm and introduce a strongly interacting component. Moreover, the apparent MD signals observed in brake pad residues in the Sheikh et al. (2022) study were caused by the presence of metallic particles in vortex states, which produce a distinctive combination of high coercivity ridge signals and low coercivity, vertically spread signals (Lappe et al., 2013). In Manchester roadside samples, we do observe some vertical spreading of contours along the B_u axis that can be attributed to particles at the upper end of the vortex size range, with some samples (e.g., BP and CP in Fig. S7) having slightly more pronounced vertical spread at low coercivities than others, indicating a transition to more MD behaviour. The contours for playground filter (DP) and the leaf (LR02) close at lower coercivities of 30–40 mT. Essentially, all samples here indicate a characteristic tri-lobate signal that we associate with vortex states and particles that may possibly stray into the MD size range.

3.11. Two-dimensional turbulent fluid flow model

According to the turbulent model used in this study, PM concentrations of variable composition with an aerodynamic diameter of 0.01 (100) μm will decline by ~1 % (−99.9 %) between 0 and-30 m distance downwind of the tredge (Fig. 7 for FeO, Supplementary Fig. S9 for other chemical compositions). This suggests that in the playground there is very little loss of ultrafine particles from the airflow through gravitational settling. Additionally, there is very little dilution of the airborne UFP particle concentrations induced by the turbulent mixing from an initial depth h of the tredge to the depth $D/v \sim \frac{0.1\,u}{v} h$. Hence the

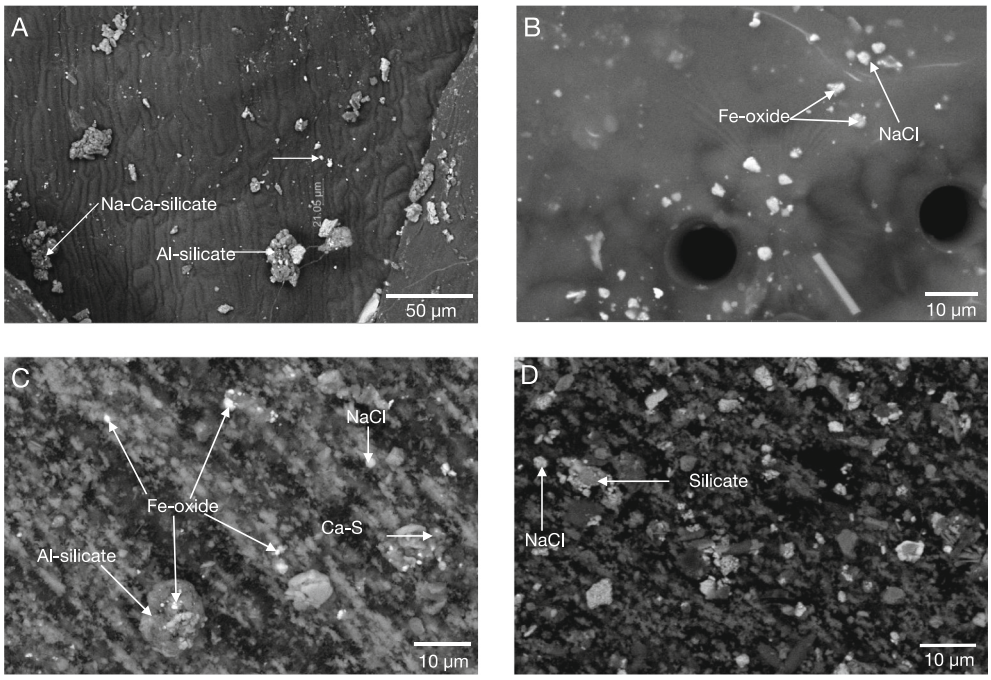

Fig. 6. Images taken using scanning electron microscopy (SEM). Backscatter electron images (BSE). A and B (Leaf); C ($PM_{2.5}$ filter); D (PM_{10} filter).

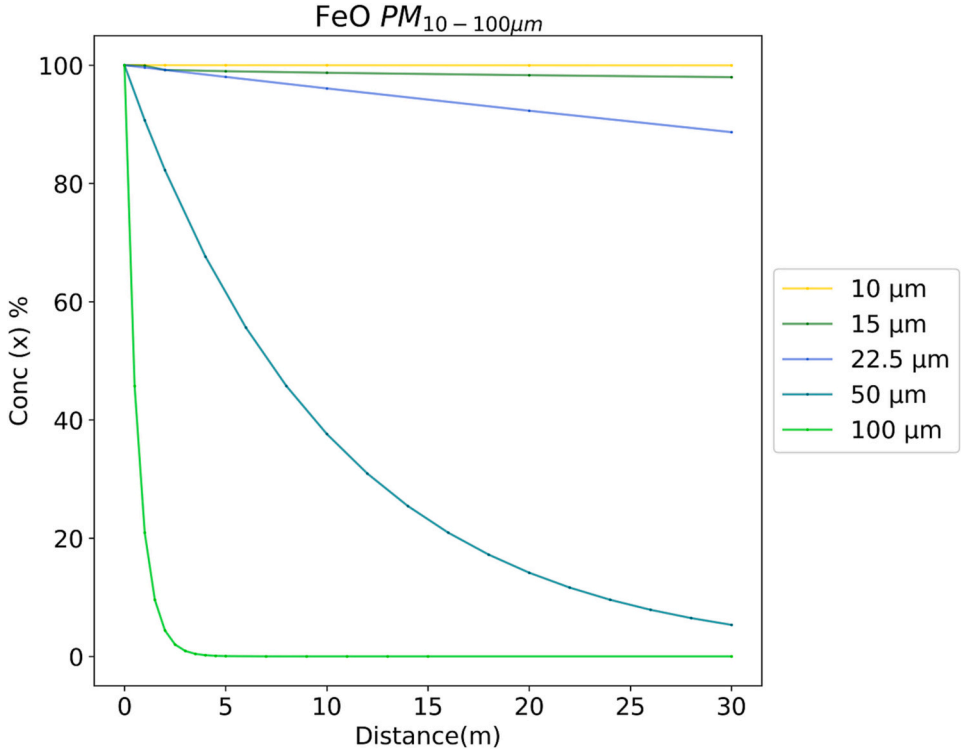

Fig. 7. Decay in concentration (%) of differently sized FeO particles with distance (m) modelled using a two-dimensional fluid flow mixing model. Particles <22.5 μm are dominated by dispersion processes while particles >22.5 μm are dominated by settling processes.

concentration of isolated UFP particles will show negligible reduction, via either settling or dispersion, in the air between the roadside source and the back of the playground (30 m from the roadside). Indeed, PM would have to be larger than ~10 μm for settling and particle dispersion to result in a substantial reduction in PM concentrations across the 30 m distance here.

3.12. Permeability of the tredge: CO_2 tracer experiment

We assessed the permeability of the tredge by releasing pulses of fire extinguisher CO_2 and then monitoring CO_2 levels within and through the tredge (Supplementary Fig. S3). 18 pulses were released both perpendicular and parallel to the tredge, and the subsequent spreading of this tracer measured over time. The monitors detected flow of the tracer

through the tredge. First arrival times (T_A) of the CO_2 gas across the tredge varied between 3 and 5 s for all the pulses fired parallel to the tredge (AA′ and CC′); and 2–4 s for the pulses fired perpendicular to the tredge (DD′, EE′, or FF′).

The mean travel speed after firing a pulse to first detection (at monitors along the plane) was around 0.5 m/s. The pulse then enters the tredge where the monitors (at 1.1 m height) detected CO_2 tracer at different times, suggestive of flow mixing within the tredge. The monitors at the top (1.7 m height) of the tredge (25, 14, and 16) detected the signal later than monitors in the middle of the tredge.

The mean travel speed decreased further when the tracer CO_2 gas travelled from roadside to school side through the tredge. This was calculated by subtracting the T_A (s) at school side monitors with T_A (s) from the tredge monitors, and using the shortest distance between the two monitors, giving mean travel speed of around 0.06 m/s.

The magnitude of the initial CO_2 pulse was highest when fired perpendicular to the tredge. In contrast, where the pulse was fired parallel to the tredge, the signal was rapidly more diluted, partly because of dispersion caused by wind (see rose diagram, Supplementary Fig. S10).

Fundamentally, these data demonstrate qualitatively that the tredge is permeable to airflow to a certain extent but sufficiently slowly permeable to cause deflection of some air over the tredge. This means that airflow through the tredge allows for 'slow filtering' and deposition of particles on the leaves through diffusion (discussed in detail later). However, quantification of any differences in mean travel speed of the tracer upon reaching the tredge (0.5 m/s) vs. its transport through the tredge and arrival at the school side (0.06 m/s) is prone to large human reaction error as T_A (s) were recorded using a stopwatch. Further, there are insufficient data to identify whether the mixing within the tredge reflects the ambient wind speed or the transport speed (i.e., vehicles generating eddy currents when moving around the S—N direction) (Supplementary Figs. S1, S10).

4. Discussion

4.1. Spatial variation in PM concentration

Gravimetric PM_{10} concentration reductions of 9–16 % were observed at Site C and Site D compared with roadside Site B. Notwithstanding the uncertainty in local background PM concentrations, the efficacy of the tredge in reducing the contribution from local, traffic-derived PM can be assessed. Taking at face value the background PM_{10} concentration from the Manchester Supersite (see methods) of 15 μg/m^3, a drop of up to 50 % in local, traffic-derived PM can be estimated between Site B and D. Our data and modelling show that this reduction arises from two mechanisms: principally a) the deposition of PM on tredge leaves (as shown in Fig. 4 and Supplementary Table S4) and b) a very minor reduction arising from turbulent mixing of particle-enriched air with 'cleaner', background air in the wake of the tredge (Fig. 7 and Supplementary Fig. S2).

In our heuristic fluid flow model, we assume that some of the air will be deflected over the tredge and will cause eddies downwind of the tredge. The mixing model shows that particle concentrations below a certain size (~<22.5 μm) and density are not governed by Stokes' settling and that the dominant airflow effect of the tredge is the turbulent mixing that occurs in its wake. Given the simplicity of the model and its underlying assumptions, we consider the predicted values of the dispersion-related drop in PM concentrations from roadside to back of the playground order-of-magnitude estimates only. The model predicts ≪1 % reduction in PM_{10} at 1 m distance from the roadside (i.e., behind the tredge, whereas, the measured reduction is 9 %). The larger-than-predicted reduction in PM_{10} indicates the removal of airborne particles through their deposition on the tredge leaves. At 30 m distance (i.e., the back of the playground), the modelled PM_{10} reduction from dispersion is <10 %, similar to the measured reduction, 7.6 %.

However, gravimetric methods are not ideally suited to monitor the local, traffic-derived PM, which is dominated by ultrafine particles that contribute greatly to the number concentration but little to the mass concentration. Magnetic measurements, on the other hand, comprise a more targeted proxy due to the Fe-oxide-rich, ultrafine nature of traffic-derived PM emissions (e.g., Gonet et al., 2021a).

4.2. SP fraction estimation

Our air-volume-normalised M_s data (Fig. 3) are a better proxy than previously used RT-SIRM proxy (Hansard et al., 2011, 2012; Hofman et al., 2014b; Maher et al., 2008, 2013; Mitchell et al., 2010; Mitchell and Maher, 2009) as they are faster and increasingly more widely available and can measure the total ferrimagnetic signal across all ferrimagnetic grain sizes, even sub-5 nm particles. In traffic-related PM, the SP fraction constitutes a significant proportion of the total magnetic PM fraction, and therefore, needs to be quantified. We observe the cumulative LT-M_s at 300 K (PM_{10} + $PM_{2.5}$) value decreases by 48 % and 67 % at the school side of tredge and playground, respectively, compared with the roadside of the tredge (Fig. 3E). Moreover, the drop in magnetic loading between the front (Site C) and the back of the playground (Site D) is far greater (31 %) is than would be predicted based on the presence of isolated magnetic particles in the SP size range (Fig. 7). This observation implies that any settling of magnetic PM observed between the school side of the tredge, and the back of the playground is due to either agglomeration of UFPs to make larger clusters and/or to the attachment of UFPs to the surfaces of much larger particles (Fig. S8).

4.3. PM deposition on leaves

Fig. 3A shows a ~40 % drop in magnetic loading (M_s at 300 K for PM_{10}) between the roadside and school side of the tredge (i.e., over ~1 m distance), followed by a further 63 % drop between the front and back of playground, giving a combined drop of ~78 % in total magnetic loading. The 40 % drop over ~1 m is far greater than expected due to dispersion alone (<1 %; Fig. 7) and is attributed to deposition of particles on the tredge leaves. The drop in magnetic loading between the roadside and the school side is even more pronounced in the magnetic $PM_{2.5}$ fraction (82 %). This hints at a preferential attraction of ultrafine particles to leaf surfaces, suggesting greater ultrafine particle deposition or adsorption by leaves, as previously reported by (Wang et al., 2019). We believe that the efficient deposition of the sub-5 nm particles is dominated by diffusional processes and cannot be due to inertial or gravitational setting as they have so little mass. The deposition on leaves can be seen as analogous to deposition of inhaled PM in the respiratory tract. The typical diffusion distances for nanoparticles can be calculated based on the diffusion coefficient determined by the Stokes-Einstein equation (Hussain et al., 2011; Zhang and Kleinstreuer, 2004) (Supplementary Text S1). We know from these equations that the diffusion length for smaller particles is greater, and if the gap between leaves is smaller (dependent on leaf density), there is a higher probability for the particles to be deposited. For example, for a diffusion length $(2*D*t)^{1/2}$ (Supplementary Text S1); assuming a particle spends around 10 s inside the tredge (an approximation based on the slowdown of CO_2 tracer velocity inside the tredge, likely influenced by wind speed and different leaf density), diffusion length (distances) for 1 nm particles are of the order 1 cm for a 10 s residence time, 0.1 cm for 10 nm particles and 0.01 cm for 100 nm particles. Where the diffusion length approaches the distances/gaps between leaf surfaces, the deposition efficiency approaches 100 %. Therefore, in this particle range we would expect a) efficient deposition overall, b) 100 % deposition of the very fine particles, and c) <100 % deposition of >5 nm particles. This is in agreement with previous studies which found that the PM contributions of PM_1 > $PM_{2.5–1}$ > $PM_{10–2.5}$, accounted for 66 %, 29 % and 5 % of the total deposited particles on leaves (Abhijith and Kumar, 2020), or that 96 % of the particles deposited on leaves were <2.5 μm (Song et al., 2015).

Moreover, assuming that the magnetic signal is mostly traffic-derived, as supported by the Fe-oxide particle size and morphology (<1 μm, aspect ratio = 0.9, Supplementary Table S3) observed by SEM and TEM, our magnetic measurements demonstrate that removal of ultrafine, traffic-derived PM by deposition on the tredge is highly efficient. This conclusion is strongly supported by the accompanying changes in M_{rs}/M_s observed at 5 K (Fig. 3). The majority (>90 %) of Fe-oxide particles in these samples are SP at room temperature. At 5 K, however, we would expect most of these particles to be below their blocking temperature and therefore to behave as stable single-domain particles with $M_{rs}/M_s \geq 0.5$. The low values of $M_{rs}/M_s = 0.08–0.3$ (Fig. 3) in the roadside $PM_{2.5}$ fraction at 5 K can be explained if ~40–80 % of the magnetic signal is carried by particles <5 nm in size; i.e., that are still in an SP state at 5 K (Dunlop, 2002). The prolific presence of sub-5 nm PM in our roadside samples is consistent with a recent air pollution study in London (Muxworthy et al., 2022) which found that up to 40 % of the magnetic signal at 10 K arises from sub-4 nm particles in size. The 82 % drop in magnetic loading observed in the $PM_{2.5}$ fraction on the school side of the tredge is accompanied by an increase in M_{rs}/M_s to ideal single-domain values (>0.5), consistent with the complete removal of the sub-5 nm fraction (as well as a proportion of the >5 nm larger single-domain particles). This observation demonstrates unequivocally that deposition, rather than dispersion, is responsible for the large drop in concentration of ultrafine traffic-related PM (dispersion would reduce magnetic loading without impacting M_{rs}/M_s). Direct observation of abundant Fe-oxide particles in the sub-5 nm size range of the roadside PM is provided in Fig. 5. A return to roadside values of both magnetic loading and M_{rs}/M_s in the $PM_{2.5}$ fraction at the back of the playground provides strong evidence for some direct mixing of roadside air with playground air at increased distance from the tredge. It is possible that there is a fresh supply of traffic PM travelling over and/or through the gap in the tredge (Fig. S1, Site A). Previous roadside studies (e.g., (Davison et al., 2009) have similarly identified highest particle number concentration (PNC) tens of metres away from a busy road. These authors also observed that the PNC peak coincided with an increase in <50 nm particles. Although some traffic-derived PM makes its way over the tredge (and/or through the tredge gap) to the back of the playground, the overall ~64–67 % reduction in total magnetic loading in the playground (Fig. 3E, F) represents a remarkable degree of protection given the simplicity, speed, and low cost of installing GI. Our magnetic methods provide a targeted means to test the spatial efficacy of GI in reducing exposure to the ultrafine fraction of local, traffic-derived PM, which could lead to improvements in design and implementation of GI in the future.

4.4. Temporal variation of magnetic PM

Based on the leaf magnetic loading results, PM deposition on leaves registered an increase between Monday (when the tredge was artificially washed) and Wednesday (Fig. 4A), confirming deposition of magnetic nanoparticles from the locally derived traffic source. Using the leaf magnetic data, around 23 % of local, traffic-derived PM_{10} is removed by deposition on the tredge, consistent with previous estimates of 7–29 % (Maher et al., 2022). This approximation is consistent with the magnitude of the drop in PM_{10} magnetic loading of the filter samples on either side of the tredge. It is important to note that % removal of PM is an estimate, and only tell us about the pollution that is removed from air passing through the vegetation and nothing about whether the PM-laden air either moves through the vegetation or around it (Pearce et al., 2021). However, our permeability experiment, using CO_2 as a tracer, confirms that the tredge is permeable enough to allow 'slow filtering' and subsequent deposition of locally sourced anthropogenic particles on leaves. After a rainfall event on Wednesday morning, it is likely that some of the leaf-deposited PM accumulated over two days was washed off the leaf surface, lowering the RT-SIRM/area signal (Fig. 4B) as observed in previous studies (Matzka and Maher, 1999; McIntosh et al., 2007; Mitchell and Maher, 2009; Mitchell et al., 2010). Just two roadside hedge locations (DR, LR) saw a moderate increase (10 % and 15 %, respectively) in magnetic loading after the rain event, perhaps indicating throughfall and localised magnetic PM redistribution as well as wash-off. Our data also suggest that 7 h of rain was much more efficient at removing magnetic PM deposited on leaves' surface than our initial 5 min washing with a hosepipe (which lowered RT-SIRM signal between 7 and 31 %); we infer a rain-induced reduction in the leaf SIRM signal by up to 70 % or more (approximate indication by dashed line, Fig. 4B) as previously reported in different studies (Mitchell and Maher, 2009; Xu et al., 2017). Moreover, removal of different-sized PM by rainfall has been studied; it has been argued that rain mostly removes larger PM (10–100 μm), followed by coarse PM (2.5–10 μm), and fine PM (0.2–2.5 μm) (Przybysz et al., 2014).

5. Conclusions

The efficient deposition of locally derived airborne PM on the leaves of a recently installed tredge of western red cedar (Maher et al., 2022) is confirmed here by PM and magnetic data and microscopy observations. We estimate that the tredge removes ~23 % of the locally derived PM_{10}. PM deposition on the tredge leaves is independently evidenced by reduced PM_{10} mass concentrations and a substantial decline in PM magnetic signal immediately behind the tredge and at the playground. These reductions in magnetic signal are especially obvious from the M_s proxy (complemented by both the RT-SIRM and LT-SIRM data) as measured behind the tredge and in the playground compared with the roadside. Mass concentrations of PM_{10} and $PM_{2.5}$ were reduced slightly behind the tredge but ultrafine (<100 nm), traffic-derived magnetic particles are reduced substantially by the tredge. This indicates efficient removal of ultrafine traffic-derived, magnetic particles by the tredge. Preferential removal of the very finest (<5 nm) particles is explained by a diffusional capture mechanism, a result of the combination of increased residence time for air within the tredge and the availability of depositional surfaces that are within easy reach of the diffusion distance. The mechanism dominantly responsible for the reduced magnetic PM signal is PM deposition on leaves, combined with a very small reduction in particle concentrations arising from particle dispersion resulting from eddy currents generated by the tredge. The slight increase in RT-SIRM value at the playground (Site D) compared with behind the tredge (Site C) (Fig. 3) can be explained by a sustained source of traffic-related magnetic PM making its way either up and over and/or through the gap in the installed tredge (see abstract graphical summary).

Our results confirm that properly designed tredges (i.e., in terms of species, leaf density, V_d, permeability, height) installed close to the locally derived PM source can effectively, rapidly, and cost-effectively mitigate exposure to airborne PM. This finding has major significance and value in reducing the present-day exposure of young children, who are especially vulnerable, to the deleterious health impacts of traffic-derived PM.

CRediT authorship contribution statement

HAS, BAM, RJH contributed to conception and design of the study. Investigation and Data curation: HAS. Formal experiments: HAS, PYT. Methodology: HAS, BAM, AWW, RJH. Validation: HAS, RJH, AWW. Visualisation: HAS, RJH. Project Administration: HAS, RJH, BAM. HAS wrote the original draft, which was reviewed and edited by RJH, BAM, and AWW. RJH supervised the project. Funding: HAS, RJH. All authors contributed to manuscript revision, read, and approved the submitted version.

Declaration of competing interest

The authors declare that they have no known competing financial interests or personal relationships that could have appeared to influence

the work reported in this paper.

Data availability

Data will be made available on request.

Acknowledgements

We would like to thank Dr Vassil Karloukovski for his unconditional support in setting up the air pumps at the school, Gary Cooper at St Ambrose's School who made sure we had all the logistical support. H.A Sheikh extends thanks to Fakhri Bintang who came all the way to Manchester to help with conducting the CO_2 tredge permeability experiment. H.A Sheikh also appreciates help from Dr Iris Buisman in booking microscopy facilities at Department of Earth Sciences. H.A Sheikh also thanks Dr Cheng Liu at Maxwell Center. H.A Sheikh and A.W Woods appreciate Dr Gennaro Dello Ioio for providing CO_2 monitors. H.A Sheikh appreciates A.A Sheikh's help in carrying heavy fire extinguishers and equipment to the school. MPMS measurements were made using Royce equipment at Cambridge Royce facilities grant EP/P024947/1 and Sir Henry Royce Institute – recurrent grant EP/R00661X/1. H.A Sheikh would like to thank the Cambridge Trust for PhD funding. P.T. and R.H. acknowledge funding by the Electron and X-ray microscopy Community for structural and chemical Imaging Techniques for Earth materials (EXCITE) (award number - G106564).

Appendix A. Supplementary data

Supplementary data to this article can be found online at https://doi.org/10.1016/j.scitotenv.2023.166598.

References

Abhijith, K.V., Kumar, P., 2019. Field investigations for evaluating green infrastructure effects on air quality in open-road conditions. Atmos. Environ. 201, 132–147. https://doi.org/10.1016/j.atmosenv.2018.12.036.

Abhijith, K.V., Kumar, P., 2020. Quantifying particulate matter reduction and their deposition on the leaves of green infrastructure. Environ. Pollut. 265, 114884 https://doi.org/10.1016/j.envpol.2020.114884.

Abhijith, K.V., Kumar, P., Gallagher, J., McNabola, A., Baldauf, R., Pilla, F., Broderick, B., Di Sabatino, S., Pulvirenti, B., 2017. Air pollution abatement performances of green infrastructure in open road and built-up street canyon environments – a review. Atmos. Environ. 162, 71–86. https://doi.org/10.1016/j.atmosenv.2017.05.014.

Al-Dabbous, A.N., Kumar, P., 2014. The influence of roadside vegetation barriers on airborne nanoparticles and pedestrians exposure under varying wind conditions. Atmos. Environ. 90, 113–124. https://doi.org/10.1016/j.atmosenv.2014.03.040.

Allen, A.G., Dick, A.L., Davison, B.M., 1997. Sources of atmospheric methanesulphonate, non-sea-salt sulphate, nitrate and related species over the temperate South Pacific. Atmos. Environ. 31, 191–205. https://doi.org/10.1016/1352-2310(96)00194-X.

Anderson, J.O., Thundiyil, J.G., Stolbach, A., 2012. Clearing the air: a review of the effects of particulate matter air pollution on human health. J. Med. Toxicol. 8, 166–175. https://doi.org/10.1007/s13181-011-0203-1.

Beckett, K.P., Freer-Smith, P.H., Taylor, G., 2000. Particulate pollution capture by urban trees: effect of species and windspeed: particulate pollution uptake by trees. Glob. Chang. Biol. 6, 995–1003. https://doi.org/10.1046/j.1365-2486.2000.00376.x.

Birmili, W., Allen, A.G., Bary, F., Harrison, R.M., 2006. Trace metal concentrations and water solubility in size-fractionated atmospheric particles and influence of road traffic. Environ. Sci. Technol. 40, 1144–1153. https://doi.org/10.1021/es0486925.

Brook, R.D., Rajagopalan, S., Pope, C.A., Brook, J.R., Bhatnagar, A., Diez-Roux, A.V., Holguin, F., Hong, Y., Luepker, R.V., Mittleman, M.A., Peters, A., Siscovick, D., Smith, S.C., Whitsel, L., Kaufman, J.D., 2010. Particulate matter air pollution and cardiovascular disease: an update to the scientific statement from the American Heart Association. Circulation 121, 2331–2378. https://doi.org/10.1161/CIR.0b013e3181dbece1.

Buccolieri, R., Salim, S.M., Leo, L.S., Di Sabatino, S., Chan, A., Ielpo, P., de Gennaro, G., Gromke, C., 2011. Analysis of local scale tree–atmosphere interaction on pollutant concentration in idealized street canyons and application to a real urban junction. Atmos. Environ. 45, 1702–1713. https://doi.org/10.1016/j.atmosenv.2010.12.058.

Chen, J., Hoek, G., 2020. Long-term exposure to PM and all-cause and cause-specific mortality: a systematic review and meta-analysis. Environ. Int. 143, 105974 https://doi.org/10.1016/j.envint.2020.105974.

Chen, X., Pei, T., Zhou, Z., Teng, M., He, L., Luo, M., Liu, X., 2015. Efficiency differences of roadside greenbelts with three configurations in removing coarse particles (PM10): a street scale investigation in Wuhan, China. Urban For. Urban Green. 14, 354–360. https://doi.org/10.1016/j.ufug.2015.02.013.

Chen, H., Kwong, J.C., Copes, R., Tu, K., Villeneuve, P.J., van Donkelaar, A., Hystad, P., Martin, R.V., Murray, B.J., Jessiman, B., Wilton, A.S., Kopp, A., Burnett, R.T., 2017. Living near major roads and the incidence of dementia, Parkinson's disease, and multiple sclerosis: a population-based cohort study. Lancet Lond. Engl. 389, 718–726. https://doi.org/10.1016/S0140-6736(16)32399-6.

Cushman-Roisin, B., Beckers, J.M., 2011. Introduction to Geophysical Fluid Dynamics: Physical and Numerical Aspects. Academic press.

Davison, B., Whyatt, D., Boardman, C., 2009. Aerosol evolution from a busy road in north-West England. Meteorol. Z. 18, 55–60. https://doi.org/10.1127/0941-2948/2008/0311.

Delgado-Saborit, J.M., Guercio, V., Gowers, A.M., Shaddick, G., Fox, N.C., Love, S., 2021. A critical review of the epidemiological evidence of effects of air pollution on dementia, cognitive function and cognitive decline in adult population. Sci. Total Environ. 757, 143734 https://doi.org/10.1016/j.scitotenv.2020.143734.

Department for Environment, Food & Rural Affairs, 2022. Concentrations of Particulate Matter (PM10 and PM2.5).

Deshmukh, P., Isakov, V., Venkatram, A., Yang, B., Zhang, K.M., Logan, R., Baldauf, R., 2019. The effects of roadside vegetation characteristics on local, near-road air quality. Air Qual. Atmos. Health 12, 259–270. https://doi.org/10.1007/s11869-018-0651-8.

Dockery, D.W., Pope, C.A., 1994. Acute respiratory effects of particulate air pollution. Annu. Rev. Public Health 15, 107–132. https://doi.org/10.1146/annurev.pu.15.050194.000543.

Dominici, F., Peng, R.D., Bell, M.L., Pham, L., McDermott, A., Zeger, S.L., Samet, J.M., 2006. Fine particulate air pollution and hospital admission for cardiovascular and respiratory diseases. JAMA 295, 1127. https://doi.org/10.1001/jama.295.10.1127.

Dunlop, D.J., 2002. Theory and application of the Day plot (M_{rs} / M_s versus H_{cr} / H_c) 2. Application to data for rocks, sediments, and soils. J. Geophys. Res. 107, 2057. https://doi.org/10.1029/2001JB000487.

Egli, R., 2013. VARIFORC: an optimized protocol for calculating non-regular first-order reversal curve (FORC) diagrams. Glob. Planet. Chang. 110, 302–320. https://doi.org/10.1016/j.gloplacha.2013.08.003.

Foitzik, M.-J., Unrau, H.-J., Gauterin, F., Dörnhöfer, J., Koch, T., 2018. Investigation of ultra fine particulate matter emission of rubber tires. Wear 394–395, 87–95. https://doi.org/10.1016/j.wear.2017.09.023.

Fussell, J.C., Franklin, M., Green, D.C., Gustafsson, M., Harrison, R.M., Hicks, W., Kelly, F.J., Kishta, F., Miller, M.R., Mudway, I.S., Oroumiyeh, F., Selley, L., Wang, M., Zhu, Y., 2022. A review of road traffic-derived non-exhaust particles: emissions, physicochemical characteristics, health risks, and mitigation measures. Environ. Sci. Technol. 56, 6813–6835. https://doi.org/10.1021/acs.est.2c01072.

Gago, E.J., Roldan, J., Pacheco-Torres, R., Ordóñez, J., 2013. The city and urban heat islands: a review of strategies to mitigate adverse effects. Renew. Sust. Energ. Rev. 25, 749–758. https://doi.org/10.1016/j.rser.2013.05.057.

Gallagher, J., Baldauf, R., Fuller, C.H., Kumar, P., Gill, L.W., McNabola, A., 2015. Passive methods for improving air quality in the built environment: a review of porous and solid barriers. Atmos. Environ. 120, 61–70. https://doi.org/10.1016/j.atmosenv.2015.08.075.

Gietl, J.K., Lawrence, R., Thorpe, A.J., Harrison, R.M., 2010. Identification of brake wear particles and derivation of a quantitative tracer for brake dust at a major road. Atmos. Environ. 44, 141–146. https://doi.org/10.1016/j.atmosenv.2009.10.016.

Gonet, T., Maher, B.A., 2019. Airborne, vehicle-derived Fe-bearing nanoparticles in the urban environment: a review. Environ. Sci. Technol. 53, 9970–9991. https://doi.org/10.1021/acs.est.9b01505.

Gonet, T., Maher, B.A., Kukutschová, J., 2021a. Source apportionment of magnetite particles in roadside airborne particulate matter. Sci. Total Environ. 752, 141828 https://doi.org/10.1016/j.scitotenv.2020.141828.

Gonet, T., Maher, B.A., Nyirő-Kósa, I., Pósfai, M., Vaculík, M., Kukutschová, J., 2021b. Size-resolved, quantitative evaluation of the magnetic mineralogy of airborne brake-wear particulate emissions. Environ. Pollut. 288, 117808 https://doi.org/10.1016/j.envpol.2021.117808.

Gustafsson, M., Blomqvist, G., Gudmundsson, A., Dahl, A., Swietlicki, E., Bohgard, M., Lindbom, J., Ljungman, A., 2008. Properties and toxicological effects of particles from the interaction between tyres, road pavement and winter traction material. Sci. Total Environ. 393, 226–240. https://doi.org/10.1016/j.scitotenv.2007.12.030.

Hagler, G.S.W., Lin, M.-Y., Khlystov, A., Baldauf, R.W., Isakov, V., Faircloth, J., Jackson, L.E., 2012. Field investigation of roadside vegetative and structural barrier impact on near-road ultrafine particle concentrations under a variety of wind conditions. Sci. Total Environ. 419, 7–15. https://doi.org/10.1016/j.scitotenv.2011.12.002.

Hammond, J., Maher, B.A., Gonet, T., Bautista, F., Allsop, D., 2022. Oxidative stress, cytotoxic and inflammatory effects of urban ultrafine road-deposited dust from the UK and Mexico in human epithelial lung (Calu-3) cells. Antioxidants 11, 1814. https://doi.org/10.3390/antiox11091814.

Hansard, R., Maher, B.A., Kinnersley, R., 2011. Biomagnetic monitoring of industry-derived particulate pollution. Environ. Pollut. 159, 1673–1681. https://doi.org/10.1016/j.envpol.2011.02.039.

Hansard, R., Maher, B.A., Kinnersley, R.P., 2012. Rapid magnetic biomonitoring and differentiation of atmospheric particulate pollutants at the roadside and around two major industrial sites in the U.K. Environ. Sci. Technol. 46, 4403–4410. https://doi.org/10.1021/es203275r.

Harrison, R.J., Feinberg, J.M., 2008. FORCinel: an improved algorithm for calculating first-order reversal curve distributions using locally weighted regression smoothing: FORCINEL ALGORITHM. Geochem. Geophys. Geosyst. 9 https://doi.org/10.1029/2008GC001987 (n/a-n/a).

Harrison, R.M., Vu, T.V., Jafar, H., Shi, Z., 2021. More mileage in reducing urban air pollution from road traffic. Environ. Int. 149, 106329 https://doi.org/10.1016/j.envint.2020.106329.

Hicks, W., Beevers, S., Tremper, A.H., Stewart, G., Priestman, M., Kelly, F.J., Lanoisellé, M., Lowry, D., Green, D.C., 2021. Quantification of non-exhaust particulate matter traffic emissions and the impact of COVID-19 lockdown at London Marylebone road. Atmosphere 12, 190. https://doi.org/10.3390/atmos12020190.

Hofman, J., Wuyts, K., Van Wittenberghe, S., Brackx, M., Samson, R., 2014a. On the link between biomagnetic monitoring and leaf-deposited dust load of urban trees: relationships and spatial variability of different particle size fractions. Environ. Pollut. 189, 63–72. https://doi.org/10.1016/j.envpol.2014.02.020.

Hofman, J., Wuyts, K., Van Wittenberghe, S., Samson, R., 2014b. On the temporal variation of leaf magnetic parameters: seasonal accumulation of leaf-deposited and leaf-encapsulated particles of a roadside tree crown. Sci. Total Environ. 493, 766–772. https://doi.org/10.1016/j.scitotenv.2014.06.074.

Hussain, M., Madl, P., Khan, P., 2011. Lung Deposition Predictions of Airborne Particles and the Emergence of Contemporary Diseases, Part-I, 2, pp. 51–59.

Irga, P.J., Burchett, M.D., Torpy, F.R., 2015. Does urban forestry have a quantitative effect on ambient air quality in an urban environment? Atmos. Environ. 120, 173–181. https://doi.org/10.1016/j.atmosenv.2015.08.050.

Janhäll, S., 2015. Review on urban vegetation and particle air pollution – deposition and dispersion. Atmos. Environ. 105, 130–137. https://doi.org/10.1016/j.atmosenv.2015.01.052.

Jeanjean, A.P.R., Hinchliffe, G., McMullan, W.A., Monks, P.S., Leigh, R.J., 2015. A CFD study on the effectiveness of trees to disperse road traffic emissions at a city scale. Atmos. Environ. 120, 1–14. https://doi.org/10.1016/j.atmosenv.2015.08.003.

Jeanjean, A.P.R., Monks, P.S., Leigh, R.J., 2016. Modelling the effectiveness of urban trees and grass on PM2.5 reduction via dispersion and deposition at a city scale. Atmos. Environ. 147, 1–10. https://doi.org/10.1016/j.atmosenv.2016.09.033.

Kremer, P., Andersson, E., McPhearson, T., Elmqvist, T., 2015. Advancing the frontier of urban ecosystem services research. Ecosyst. Serv. 12, 149–151. https://doi.org/10.1016/j.ecoser.2015.01.008.

Kukutschová, J., Moravec, P., Tomášek, V., Matějka, V., Smolík, J., Schwarz, J., Seidlerová, J., Šafářová, K., Filip, P., 2011. On airborne nano/micro-sized wear particles released from low-metallic automotive brakes. Environ. Pollut. 159, 998–1006. https://doi.org/10.1016/j.envpol.2010.11.036.

Kumar, P., Valappil, Abhijith Kooloth, Barwise, Yendle, 2019a. Implementing Green Infrastructure for Air Pollution Abatement: General Recommendations for Management and Plant Species Selection. figshare. https://doi.org/10.6084/M9.FIGSHARE.8198261.V4.

Kumar, P., Druckman, A., Gallagher, J., Gatersleben, B., Allison, S., Eisenman, T.S., Hoang, U., Hama, S., Tiwari, A., Sharma, A., Abhijith, K.V., Adlakha, D., McNabola, A., Astell-Burt, T., Feng, X., Skeldon, A.C., De Lusignan, S., Morawska, L., 2019b. The nexus between air pollution, green infrastructure and human health. Environ. Int. 133, 105181 https://doi.org/10.1016/j.envint.2019.105181.

Kupiainen, K.J., Tervahattu, H., Räisänen, M., Mäkelä, T., Aurela, M., Hillamo, R., 2005. Size and composition of airborne particles from pavement wear, tires, and traction sanding. Environ. Sci. Technol. 39, 699–706. https://doi.org/10.1021/es035419e.

Lanci, L., Kent, D.V., 2018. Forward modeling of thermally activated single-domain magnetic particles applied to first-order reversal curves. J. Geophys. Res. Solid Earth 123, 3287–3300. https://doi.org/10.1002/2018JB015463.

Lappe, S.L.L., Feinberg, J.M., Muxworthy, A., Harrison, R.J., 2013. Comparison and calibration of nonheating paleointensity methods: a case study using dusty olivine. Geochem. Geophys. Geosyst. 14, 2143–2158. https://doi.org/10.1002/ggge.20141.

Lee, A.C.K., Maheswaran, R., 2011. The health benefits of urban green spaces: a review of the evidence. J. Public Health 33, 212–222. https://doi.org/10.1093/pubmed/fdq068.

Leitte, A.M., Schlink, U., Herbarth, O., Wiedensohler, A., Pan, X.-C., Hu, M., Wehner, B., Breitner, S., Peters, A., Wichmann, H.-E., Franck, U., 2012. Associations between size-segregated particle number concentrations and respiratory mortality in Beijing, China. Int. J. Environ. Health Res. 22, 119–133. https://doi.org/10.1080/09603123.2011.605878.

Maher, B.A., 1988. Magnetic properties of some synthetic sub-micron magnetites. Geophys. J. Int. 94, 83–96. https://doi.org/10.1111/j.1365-246X.1988.tb03429.x.

Maher, B.A., Moore, C., Matzka, J., 2008. Spatial variation in vehicle-derived metal pollution identified by magnetic and elemental analysis of roadside tree leaves. Atmos. Environ. 42, 364–373. https://doi.org/10.1016/j.atmosenv.2007.09.013.

Maher, B.A., Ahmed, I.A.M., Davison, B., Karloukovski, V., Clarke, R., 2013. Impact of roadside tree lines on indoor concentrations of traffic-derived particulate matter. Environ. Sci. Technol. 47, 13737–13744. https://doi.org/10.1021/es404363m.

Maher, B.A., Gonet, T., Karloukovski, V.V., Wang, H., Bannan, T.J., 2022. Protecting playgrounds: local-scale reduction of airborne particulate matter concentrations through particulate deposition on roadside 'tredges' (green infrastructure). Sci. Rep. 12, 14236. https://doi.org/10.1038/s41598-022-18509-w.

Makri, A., Stilianakis, N.I., 2008. Vulnerability to air pollution health effects. Int. J. Hyg. Environ. Health 211, 326–336. https://doi.org/10.1016/j.ijheh.2007.06.005.

Matzka, J., Maher, B.A., 1999. Magnetic biomonitoring of roadside tree leaves: identification of spatial and temporal variations in vehicle-derived particulates. Atmos. Environ. 33, 4565–4569. https://doi.org/10.1016/S1352-2310(99)00229-0.

McIntosh, G., Gómez-Paccard, M., Osete, M.L., 2007. The magnetic properties of particles deposited on Platanus x hispanica leaves in Madrid, Spain, and their temporal and spatial variations. Sci. Total Environ. 382, 135–146. https://doi.org/10.1016/j.scitotenv.2007.03.020.

Mitchell, R., Maher, B.A., 2009. Evaluation and application of biomagnetic monitoring of traffic-derived particulate pollution. Atmos. Environ. 43, 2095–2103. https://doi.org/10.1016/j.atmosenv.2009.01.042.

Mitchell, R., Maher, B.A., Kinnersley, R., 2010. Rates of particulate pollution deposition onto leaf surfaces: temporal and inter-species magnetic analyses. Environ. Pollut. 158, 1472–1478. https://doi.org/10.1016/j.envpol.2009.12.029.

Muxworthy, A.R., Lam, C., Green, D., Cowan, A., Maher, B.A., Gonet, T., 2022. Magnetic characterisation of London's airborne nanoparticulate matter. Atmos. Environ. 287, 119292 https://doi.org/10.1016/j.atmosenv.2022.119292.

Newby, D.E., Mannucci, P.M., Tell, G.S., Baccarelli, A.A., Brook, R.D., Donaldson, K., Forastiere, F., Franchini, M., Franco, O.H., Graham, I., Hoek, G., Hoffmann, B., Hoylaerts, M.F., Künzli, N., Mills, N., Pekkanen, J., Peters, A., Piepoli, M.F., Rajagopalan, S., Storey, R.F., 2015. Expert position paper on air pollution and cardiovascular disease. Eur. Heart J. 36, 83–93. https://doi.org/10.1093/eurheartj/ehu458.

Nowak, D.J., Crane, D.E., Stevens, J.C., 2006. Air pollution removal by urban trees and shrubs in the United States. Urban For. Urban Green. 4, 115–123. https://doi.org/10.1016/j.ufug.2006.01.007.

Ottosen, T.-B., Kumar, P., 2020. The influence of the vegetation cycle on the mitigation of air pollution by a deciduous roadside hedge. Sustain. Cities Soc. 53, 101919 https://doi.org/10.1016/j.scs.2019.101919.

Ozdemir, H., 2019. Mitigation impact of roadside trees on fine particle pollution. Sci. Total Environ. 659, 1176–1185. https://doi.org/10.1016/j.scitotenv.2018.12.262.

Özdemir, Ö., Dunlop, D.J., 2010. Hallmarks of maghemitization in low-temperature remanence cycling of partially oxidized magnetite nanoparticles. J. Geophys. Res. 115, B02101 https://doi.org/10.1029/2009JB006756.

Özdemir, Ö., Dunlop, D.J., Moskowitz, B.M., 1993. The effect of oxidation on the Verwey transition in magnetite. Geophys. Res. Lett. 20, 1671–1674. https://doi.org/10.1029/93GL01483.

Pankhurst, Q., Hautot, D., Khan, N., Dobson, J., 2008. Increased levels of magnetic iron compounds in Alzheimer's disease. J. Alzheimers Dis. 13, 49–52. https://doi.org/10.3233/JAD-2008-13105.

Pearce, H., Levine, J.G., Cai, X., MacKenzie, A.R., 2021. Introducing the green infrastructure for roadside air quality (GI4RAQ) platform: estimating site-specific changes in the dispersion of vehicular pollution close to source. Forests 12, 769. https://doi.org/10.3390/f12060769.

Pérez, G., Coma, J., Martorell, I., Cabeza, L.F., 2014. Vertical greenery systems (VGS) for energy saving in buildings: a review. Renew. Sust. Energ. Rev. 39, 139–165. https://doi.org/10.1016/j.rser.2014.07.055.

Peters, K., Eiden, R., 1992. Modelling the dry deposition velocity of aerosol particles to a spruce forest. Atmos. Environ. Part Gen. Top. 26, 2555–2564. https://doi.org/10.1016/0960-1686(92)90108-W.

Przybysz, A., Sæbø, A., Hanslin, H.M., Gawroński, S.W., 2014. Accumulation of particulate matter and trace elements on vegetation as affected by pollution level, rainfall and the passage of time. Sci. Total Environ. 481, 360–369. https://doi.org/10.1016/j.scitotenv.2014.02.072.

Pugh, T.A.M., MacKenzie, A.R., Whyatt, J.D., Hewitt, C.N., 2012. Effectiveness of green infrastructure for improvement of air quality in urban street canyons. Environ. Sci. Technol. 46, 7692–7699. https://doi.org/10.1021/es300826w.

Rovelli, S., Cattaneo, A., Nuzzi, C., Spinazzè, A., Piazza, S., Carrer, P., Cavallo, D., 2014. Airborne particulate matter in school classrooms of northern Italy. Int. J. Environ. Res. Public Health 11, 1398–1421. https://doi.org/10.3390/ijerph110201398.

Sagnotti, L., Macrì, P., Egli, R., Mondino, M., 2006. Magnetic properties of atmospheric particulate matter from automatic air sampler stations in Latium (Italy): toward a definition of magnetic fingerprints for natural and anthropogenic PM $_{10}$ sources: magnetic properties of atmospheric PM. J. Geophys. Res. Solid Earth 111. https://doi.org/10.1029/2006JB004508 (n/a-n/a).

Sagnotti, L., Taddeucci, J., Winkler, A., Cavallo, A., 2009. Compositional, morphological, and hysteresis characterization of magnetic airborne particulate matter in Rome, Italy: characterization of magnetic PM in ROME. Geochem. Geophys. Geosyst. 10 https://doi.org/10.1029/2009GC002563 (n/a-n/a).

Sanders, P.G., Xu, N., Dalka, T.M., Maricq, M.M., 2003. Airborne brake Wear debris: size distributions, composition, and a comparison of dynamometer and vehicle tests. Environ. Sci. Technol. 37, 4060–4069. https://doi.org/10.1021/es034145s.

Santiago, J.-L., Martilli, A., Martin, F., 2017. On dry deposition modelling of atmospheric pollutants on vegetation at the microscale: application to the impact of street vegetation on air quality. Bound.-Layer Meteorol. 162, 451–474. https://doi.org/10.1007/s10546-016-0210-5.

Santiago, J.-L., Buccolieri, R., Rivas, E., Calvete-Sogo, H., Sanchez, B., Martilli, A., Alonso, R., Elustondo, D., Santamaría, J.M., Martin, F., 2019. CFD modelling of vegetation barrier effects on the reduction of traffic-related pollutant concentration in an avenue of Pamplona, Spain. Sustain. Cities Soc. 48, 101559 https://doi.org/10.1016/j.scs.2019.101559.

Saragnese, F., Lanci, L., Lanza, R., 2011. Nanometric-sized atmospheric particulate studied by magnetic analyses. Atmos. Environ. 45, 450–459. https://doi.org/10.1016/j.atmosenv.2010.09.057.

Schulz, H., Harder, V., Ibald-Mulli, A., Khandoga, A., Koenig, W., Krombach, F., Radykewicz, R., Stampfl, A., Thorand, B., Peters, A., 2005. Cardiovascular effects of fine and ultrafine particles. J. Aerosol Med. 18, 1–22. https://doi.org/10.1089/jam.2005.18.1.

Schwartz, J., 2004. Air pollution and children's health. Pediatrics 113, 1037–1043. https://doi.org/10.1542/peds.113.S3.1037.

Seaton, A., Godden, D., MacNee, W., Donaldson, K., 1995. Particulate air pollution and acute health effects. Lancet 345, 176–178. https://doi.org/10.1016/S0140-6736(95)90173-6.

Sheikh, H.A., Maher, B.A., Karloukovski, V., Lampronti, G.I., Harrison, R.J., 2022. Biomagnetic characterization of air pollution particulates in Lahore, Pakistan. Geochem. Geophys. Geosyst. 23 https://doi.org/10.1029/2021GC010293.

Song, Y., Maher, B.A., Li, F., Wang, X., Sun, X., Zhang, H., 2015. Particulate matter deposited on leaf of five evergreen species in Beijing, China: source identification and size distribution. Atmos. Environ. 105, 53–60. https://doi.org/10.1016/j.atmosenv.2015.01.032.

Sunyer, J., Esnaola, M., Alvarez-Pedrerol, M., Forns, J., Rivas, I., López-Vicente, M., Suades-González, E., Foraster, M., Garcia-Esteban, R., Basagaña, X., Viana, M., Cirach, M., Moreno, T., Alastuey, A., Sebastian-Galles, N., Nieuwenhuijsen, M., Querol, X., 2015. Association between traffic-related air pollution in schools and cognitive development in primary school children: a prospective cohort study. PLoS Med. 12, e1001792 https://doi.org/10.1371/journal.pmed.1001792.

Tallis, M., Taylor, G., Sinnett, D., Freer-Smith, P., 2011. Estimating the removal of atmospheric particulate pollution by the urban tree canopy of London, under current and future environments. Landsc. Urban Plan. 103, 129–138. https://doi.org/10.1016/j.landurbplan.2011.07.003.

Tandon, P., Saelens, B., Zhou, C., Christakis, D., 2018. A comparison of preschoolers' physical activity indoors versus outdoors at child care. Int. J. Environ. Res. Public Health 15, 2463. https://doi.org/10.3390/ijerph15112463.

Thorpe, A., Harrison, R.M., 2008. Sources and properties of non-exhaust particulate matter from road traffic: a review. Sci. Total Environ. 400, 270–282. https://doi.org/10.1016/j.scitotenv.2008.06.007.

Tiwari, A., Kumar, P., 2022. Quantification of green infrastructure effects on airborne nanoparticles dispersion at an urban scale. Sci. Total Environ. 838, 155778 https://doi.org/10.1016/j.scitotenv.2022.155778.

Tiwari, A., Kumar, P., Kalaiarasan, G., Ottosen, T.-B., 2021. The impacts of existing and hypothetical green infrastructure scenarios on urban heat island formation. Environ. Pollut. 274, 115898 https://doi.org/10.1016/j.envpol.2020.115898.

Tomson, M., Kumar, P., Barwise, Y., Perez, P., Forehead, H., French, K., Morawska, L., Watts, J.F., 2021. Green infrastructure for air quality improvement in street canyons. Environ. Int. 146, 106288 https://doi.org/10.1016/j.envint.2020.106288.

Vos, P.E.J., Maiheu, B., Vankerkom, J., Janssen, S., 2013. Improving local air quality in cities: to tree or not to tree? Environ. Pollut. 183, 113–122. https://doi.org/10.1016/j.envpol.2012.10.021.

Wang, H., Maher, B.A., Ahmed, I.A., Davison, B., 2019. Efficient removal of ultrafine particles from diesel exhaust by selected tree species: implications for roadside planting for improving the quality of urban air. Environ. Sci. Technol. 53, 6906–6916. https://doi.org/10.1021/acs.est.8b06629.

Weichenthal, S., Pinault, L., Christidis, T., Burnett, R.T., Brook, J.R., Chu, Y., Crouse, D. L., Erickson, A.C., Hystad, P., Li, C., Martin, R.V., Meng, J., Pappin, A.J., Tjepkema, M., van Donkelaar, A., Weagle, C.L., Brauer, M., 2022. How low can you go? Air pollution affects mortality at very low levels. Sci. Adv. 8, eabo3381 https://doi.org/10.1126/sciadv.abo3381.

Weuve, J., Bennett, E.E., Ranker, L., Gianattasio, K.Z., Pedde, M., Adar, S.D., Yanosky, J. D., Power, M.C., 2021. Exposure to air pollution in relation to risk of dementia and related outcomes: an updated systematic review of the epidemiological literature. Environ. Health Perspect. 129, 096001 https://doi.org/10.1289/EHP8716.

Winkler, A., Amoroso, A., Di Giosa, A., Marchegiani, G., 2021. The effect of Covid-19 lockdown on airborne particulate matter in Rome, Italy: a magnetic point of view. Environ. Pollut. 291, 118191 https://doi.org/10.1016/j.envpol.2021.118191.

Winkler, A., Contardo, T., Lapenta, V., Sgamellotti, A., Loppi, S., 2022. Assessing the impact of vehicular particulate matter on cultural heritage by magnetic biomonitoring at Villa Farnesina in Rome, Italy. Sci. Total Environ. 823, 153729 https://doi.org/10.1016/j.scitotenv.2022.153729.

Xu, X., Zhang, Z., Bao, L., Mo, L., Yu, X., Fan, D., Lun, X., 2017. Influence of rainfall duration and intensity on particulate matter removal from plant leaves. Sci. Total Environ. 609, 11–16. https://doi.org/10.1016/j.scitotenv.2017.07.141.

Yang, A., Hellack, B., Leseman, D., Brunekreef, B., Kuhlbusch, T.A.J., Cassee, F.R., Hoek, G., Janssen, N.A.H., 2015. Temporal and spatial variation of the metal-related oxidative potential of PM 2.5 and its relation to PM 2.5 mass and elemental composition. Atmos. Environ. 102, 62–69. https://doi.org/10.1016/j.atmosenv.2014.11.053.

Zhang, L., 2001. A size-segregated particle dry deposition scheme for an atmospheric aerosol module. Atmos. Environ. 35, 549–560. https://doi.org/10.1016/S1352-2310(00)00326-5.

Zhang, Z., Kleinstreuer, C., 2004. Airflow structures and nano-particle deposition in a human upper airway model. J. Comput. Phys. 198, 178–210. https://doi.org/10.1016/j.jcp.2003.11.034.